processes

MDPI

Article

Natural Mineral Sorbents as Green Materials for the Remediation of Oil-Contaminated Waters

Dana Belgibayeva [1], Nuriya Aikenova [1,2,*], Guzel Abilova [2], Asema Biktasova [1], Gulden Lepesbayeva [1,2] and Saifulla Nazarov [3]

[1] Departament of Chemistry, Institute of Natural Sciences, L.N. Gumilyov Eurasian National University, Astana 010000, Kazakhstan; belgibayeva_ds@enu.kz (D.B.)
[2] Department of Oil and Gas Business, Laboratory of Chemistry and Ecology, Technical Faculty, K. Zhubanov Aktobe Regional University, Aktobe 030000, Kazakhstan
[3] Department of Chemistry and Oil and Gas Technology, Bukhara State University, Bukhara 200100, Uzbekistan; s.i.nazarov@buxdu.uz
* Correspondence: aikenova_nye@enu.kz; Tel.: +7-7713042210

Abstract

This study experimentally demonstrates that a bentonite–vermiculite composite (1:2 mass ratio) is the most effective formulation for the treatment of crude oil–contaminated wastewater. The sorbents were characterized using XRD, SEM/EDS, ζ-potential, DLS, and TGA/DSC to evaluate their structural, surface, and adsorption-related properties. Kinetic analysis showed that the adsorption process followed the pseudo-second-order (PSO) model (R^2 = 0.96–0.99), suggesting that surface interactions and intraparticle diffusion within the layered composite governed the overall adsorption rate. Thermodynamic analysis revealed negative Gibbs free energy values (ΔG < 0) and a moderately positive enthalpy change (ΔH ≈ 26 kJ·mol^{-1}), confirming that adsorption is spontaneous and endothermic, with contributions from physical interactions, ion exchange, and hydrophobic effects. After adsorption, the ζ-potential shifted toward less negative values, indicating partial surface charge neutralization by hydrocarbon species. TGA/DSC data further confirmed strong oil retention and preserved structural stability of the sorbents, while the DSC-derived enthalpy increased from 2.0 kJ·g^{-1} to 141.6 kJ·g^{-1} after hydrocarbon uptake, indicating pronounced energetic effects associated with sorbate incorporation. Techno-economic evaluation under industrially relevant conditions (Q = 120,000 L·h^{-1}; C_0 = 392 mg·L^{-1}) showed effective oil removal to residual concentrations below regulatory discharge limits at a low treatment cost.

Keywords: bentonite clay; vermiculite; wastewater; adsorption; green technologies

Academic Editors: Maria Jose Martin de Vidales, Leticia Nishi, Luis Fernando Cusioli, Rosângela Bergamasco and Carolina Moser Paraíso

Received: 15 December 2025
Revised: 16 January 2026
Accepted: 25 January 2026
Published: 4 February 2026

1. Introduction

Environmental contamination of water and soil with harmful substances has become an increasingly pressing global challenge. Oil and petroleum-derived products, including gasoline, diesel fuel, fuel oil, kerosene, lubricants, paraffins, and sulfates, are among the major pollutants entering natural water bodies as a result of industrial discharges associated with oil production, refining, and transportation. This issue is particularly relevant in several regions in Kazakhstan, where petroleum contamination of aquatic ecosystems has been widely reported [1]. Once released into the environment, oil and its components may exert toxic effects on living organisms, disrupt aquatic and terrestrial ecosystems, and alter the physical, chemical, and biological properties of affected environmental matrices [2].

Given that water and soil underpin habitats for plants and animals, contamination of these resources poses a substantial ecological risk.

At present, the removal of petroleum products from water remains an important scientific and practical task. Considerable research efforts have been directed toward identifying efficient and low-cost sorbent materials for the purification of oil-polluted water [3–7]. Sorption-based technologies are particularly attractive due to their operational simplicity, technical accessibility, and relatively low cost; therefore, the development of effective sorbents and optimization of sorption-based treatment processes remain highly relevant.

Natural mineral materials exhibit sorption activity even in their native state, largely owing to surface adsorption and the swelling behavior of clay-rich sedimentary minerals. However, many studies indicate that additional activation of mineral sorbents can be beneficial, as it enables tailoring of the pore structure and enhancement of the cation-exchange capacity, thereby improving adsorption performance in water treatment [1,8,9]. At the same time, the feasibility of using both natural and modified sorbents should be evaluated under environmentally realistic conditions.

A review of the scientific and patent literature suggests that one of the most promising approaches for treating wastewater contaminated with petroleum products is sorption using mineral–sedimentary materials such as zeolites and natural clays. These sorbents are relatively inexpensive, readily available, and, in many cases, suitable for reuse or safe disposal, making them economically attractive for large-scale oil-spill remediation and industrial wastewater treatment [4,5].

In this context, the present study evaluates natural mineral sorbents, including bentonite clay and vermiculite, in their raw form and after acid activation. Particular attention is paid to the effect of activation on the specific surface area and textural characteristics of the materials, as well as to their adsorption performance in removing petroleum contaminants and heavy metals from polluted water and soils.

The findings of this study are expected to contribute to the development of efficient, affordable, and environmentally sustainable sorbents suitable for practical application in petroleum-contaminated environments.

2. Materials and Methods

2.1. Materials

Iodine standard solution (0.05 N; Sigma-Aldrich, St. Louis, MO, USA), sodium thiosulfate standard solution (0.1 N; Merck, Darmstadt, Germany), potassium iodide (analytical grade; 10 wt.% aqueous solution; Sigma-Aldrich, St. Louis, MO, USA), starch indicator (1 wt.% aqueous solution; Fluka, Buchs, Switzerland), and distilled water (laboratory grade) were used for iodometric determinations. For chemical oxygen demand (COD) analysis, potassium dichromate ($K_2Cr_2O_7$), sulfuric acid (H_2SO_4), silver sulfate (Ag_2SO_4), mercury (II) sulfate ($HgSO_4$), ammonium iron(II) sulfate hexahydrate ($(NH_4)_2Fe(SO_4)_2 \cdot 6H_2O$), and 1,10-phenanthroline ($C_{12}H_8N_2$) (analytical grade; all Sigma-Aldrich, St. Louis, MO, USA) were used as received. Methylene blue ($C_{16}H_{18}ClN_3S$; analytical grade; Sigma-Aldrich, St. Louis, MO, USA) solutions were prepared in the range of 10–100 $mg \cdot L^{-1}$ using distilled water unless otherwise stated.

The bentonite clay was supplied by LLP “Tagbent” (Kamenogorsk, Kazakhstan), whose raw material base is the Taganskoe deposit located in the East Kazakhstan Region of the Kazakhstan. Expanded vermiculite was purchased from LLP “Avenue” (Kamenogorsk, Kazakhstan); its raw material base originates from the Kulantau deposit in the Tulkubas District of the Turkestan Region (Kazakhstan).

A formation water sample containing crude oil was collected from the Kumsai oil field in the Aktobe Region (Kazakhstan). The sampling date was 3 October 2023.

2.2. Experimental Methods

2.2.1. Iodine Sorption Activity

The iodine sorption activity was determined by adsorption of iodine from aqueous solution followed by iodometric titration of residual iodine with sodium thiosulfate. Briefly, a sorbent portion (m = 0.10 g) was contacted with 50.0 mL of iodine standard solution (0.05 N) and agitated on a magnetic stirrer for 30 min at room temperature (20–25 °C). The suspension was filtered, and the filtrate was titrated with sodium thiosulfate standard solution (0.1 N) in the presence of KI (10 wt.% aqueous solution) and starch indicator (1 wt.% aqueous solution) to determine the residual iodine concentration. The iodine sorption activity, A_e (mg·g^{-1}), was calculated as:

$$A_e = \frac{(C_0 - C) \cdot V \cdot M}{m} \quad (1)$$

C_0 and C are the initial and residual iodine concentrations (mol·L^{-1}), respectively; V is the solution volume (L); M is the molar mass of iodine (I_2, 253.8 g·mol^{-1}); and m is the sorbent mass (g).

2.2.2. Methylene Blue Adsorption Capacity (AMB, mg·g^{-1})

The sorption capacity toward methylene blue (MB) was determined by batch adsorption followed by UV–V is analysis of the residual dye concentration. A sorbent mass of 0.05–0.10 g was mixed with 50.0 mL of MB solution (10–100 mg·L^{-1}) and agitated for 60 min at 20–25 °C. The solid phase was separated by filtration, and the absorbance of the solution was recorded at 664 nm. Residual MB concentrations were obtained from a calibration curve. UV–Vis spectra were recorded on a ZUZI 4201/20 (Auxilab, Beriain, Spain) double-beam spectrophotometer using 10 mm quartz cuvettes. The MB uptake, A_{MB} (mg·g^{-1}), was calculated as:

$$A_{MB} = \frac{(C_0 - C) \cdot V}{m} \quad (2)$$

C_0 and C are the initial and equilibrium MB concentrations (mg·L^{-1}); V is the solution volume (L); and m is the sorbent mass (g).

2.2.3. Batch Adsorption Experiments

Prior to use, bulk adsorbent samples were dried at 120 °C for 2.5 h to remove physically adsorbed moisture Batch adsorption experiments were performed under static conditions in glass conical flasks by contacting 50.0 mL of model wastewater (pH 6.86) with 1.0 g of adsorbent. The model wastewater was prepared by dispersing 2.0 mL of a petroleum emulsion (density, 0.869 g·cm^{-3}) in 500 mL of distilled water to obtain a homogeneous oil-in-water system prior to use. The suspensions were stirred magnetically at 200 rpm for 30 min at (25 ± 2) °C. After equilibration, the solid phase was separated by vacuum filtration, and the filtrates were analyzed for residual petroleum contamination via COD (expressed as mg O_2·L^{-1}). The equilibrium adsorption capacity, qe (mg O_2·g^{-1}), was calculated according to Equation (3) following the procedure reported in [2,10]:

$$q_e = \frac{COD_0 - COD_e}{m} V \quad (3)$$

where COD_0 and $CODe$ are the initial and equilibrium COD values (mg O_2·L^{-1}), respectively; V is the solution volume (L); and m is the adsorbent mass (g); V—volume of the solution, L; m—mass of the adsorbent (g). All adsorption tests were conducted in triplicate (n = 3). The experimental results are presented as mean values accompanied by standard deviations; the relative error did not exceed 5%.

2.2.4. ζ-Potential, DLS Size, and Electrokinetic Stability Parameters (PALS/DLS)

ζ-potential measurements were performed at (25 ± 2) °C using a NanoBrook Omni analyzer (Brookhaven Instruments Co., Nashua, NH, USA) equipped with electrophoretic light scattering in phase analysis light scattering (PALS) mode and dynamic light scattering (DLS) for hydrodynamic sizing. Adsorbent suspensions were prepared in aqueous KCl solutions spanning an ionic-strength range of I = 0–1.0 M. In each experiment, 0.0010 g of adsorbent (bentonite or bentonite–vermiculite composite (1:2) was dispersed in 50.0 mL of KCl at the required concentration and homogenized to obtain a uniform suspension. The suspensions were characterized before and after sorption under the same electrolyte conditions. During suspension preparation and the sorption stage, samples were mechanically agitated on a digital orbital shaker OS-20 V.1AW (Biosan, Riga, Latvia) for 24 h at 25 °C and 150 rpm to ensure homogeneous dispersion and to approach adsorption equilibrium. All electrokinetic measurements were carried out at pH ≈ 6.0.

The ζ-potential (ζ), regarded as an operational electrokinetic parameter according to IUPAC, was calculated from the electrophoretic mobility (μ_e) using the Smoluchowski approximation (κa ≫ 1) [11–14]:

$$\zeta = \frac{\mu_0 - \eta}{\varepsilon_r \varepsilon_0} \quad (4)$$

$$\mu_e = \frac{\varepsilon_r + \varepsilon_0}{\eta} \zeta \quad (5)$$

where μ_e—electrophoretic mobility; ε_r—relative permittivity (dielectric constant) of the medium; ε_0—vacuum permittivity (electric constant); η—dynamic viscosity of the medium DLS hydrodynamic size and characteristic radius.

Hydrodynamic size was measured by dynamic light scattering (DLS) at the corresponding ionic strength (KCl = 0.001M) to assess adsorption-induced dispersion and to define the characteristic length scale for electrokinetic analysis. The characteristic aggregate radius was taken as: a = $d_h/2$. Changes in d_h before and after sorption were attributed to variations in interparticle interactions governed by electrostatic screening and surface charge state.

Double-Layer Thickness, *κa* Criterion, and Ionic-Strength Dependence

To justify the applicability of the Smoluchowski limit, the Debye length λ_D and Debye parameter κ were calculated for a symmetric 1:1 electrolyte (KCl) as:

$$\lambda_D = \left(\frac{\varepsilon_r \varepsilon_0 RT}{2F^2 L I^*} \right)^{\frac{1}{2}} \quad (6)$$

*I**—ionic strength. The dimensionless parameter:

$$ka = k \cdot a \quad (7)$$

The dimensionless parameter κa was used to assess model validity and electrokinetic stability: increasing ionic strength raises κa, reflecting diffuse-layer compression and reduced interparticle repulsion, in agreement with DLS trends.

Dukhin Number (Du) to Assess Surface-Conductivity Contributions

Because ζ is obtained from μ_e using an electrokinetic model, the potential influence of surface conductivity (conductivity of the electrical double layer) was evaluated via the Dukhin number Du [15–20]. In its general form

$$Du = \frac{k^\sigma}{k_{m^\alpha}} \quad (8)$$

κ^{σ}—surface conductivity (i.e., conductivity of the electrical double layer); κ_m—bulk electrical conductivity of the solution; α—characteristic particle size (typically the particle radius)

$$Du = \frac{2}{k_\alpha}\left(1 + \frac{3m}{z^2}\right)\left(\cosh\left(\frac{zF\zeta}{2RT}\right) - 1\right) \quad (9)$$

$$m = \frac{2\varepsilon_r\varepsilon_0 R^2T^2}{3\eta F^2 D} \quad (10)$$

D—ion diffusion coefficient (diffusion coefficient of ions).

2.3. Structural and Thermal Characterization

Structural and thermal characterization was performed to elucidate the morphology, phase composition, and thermal stability of the sorbents before and after adsorption. The composition and morphology of the mineral samples before and after sorption were examined using a ZEISS Crossbeam 540 scanning electron microscope (Carl Zeiss Microscopy GmbH, Oberkochen, Germany). Powdered samples were mounted on carbon adhesive substrates and analyzed without conductive coating at an accelerating voltage of 10–15 kV.

X-ray diffraction (XRD) analysis was carried out on a D6 PHASER diffractometer (Bruker AXS GmbH, Karlsruhe, Germany) using Cu–Kα radiation (λ = 1.5406 Å) over the 2θ range of 5–80°.

Thermogravimetric analysis (TGA) was conducted using a NETZSCH STA 449 F3 Jupiter simultaneous thermal analyzer (NETZSCH-Gerätebau GmbH, Selb, Germany); approximately 15–20 mg of sample was heated from 10 to 1300 °C at a rate of 10 °C·min^{-1} under a flowing argon atmosphere.

2.4. Adsorption Isotherm, Kinetic, and Thermodynamic Models

Adsorption isotherms (Langmuir and Freundlich) were applied to examine the relationship between the equilibrium adsorbate concentration in solution and its uptake by the adsorbent [21]. The Langmuir model assumes monolayer coverage on a homogeneous surface with a finite number of identical sites and no lateral interactions is defined by Equation (11), whereas the empirical Freundlich model describes adsorption on energetically heterogeneous surfaces and allows for multilayer uptake is articulated in Equation (12). Adsorption kinetics were evaluated using the pseudo-first-order (PFO) and pseudo-second-order (PSO) rate equations to quantify the time-dependent adsorption behavior and to identify the rate-controlling mechanism (Equations (13) and (14)) [22]. Thermodynamic parameters were determined to assess the feasibility and energetic nature of the adsorption process: the Gibbs free energy change (ΔG) was calculated from the relevant equilibrium constant, while the enthalpy (ΔH) and entropy (ΔS) changes were obtained from the slope and intercept of the Van't Hoff plot according to the Van't Hoff relationship (Equations (15) and (16)) [23].

$$Q_t = \frac{Q_{\max} K_L C_e}{1 + K_L C_e} \quad (11)$$

$$Q_e = K_f C - e^{\frac{1}{n}}. \quad (12)$$

$$Q_t = Q_t\left(1 - e^{-k_1 t}\right) \quad (13)$$

$$Q_t = \frac{k_2 Q_e^2 t}{1 + k_2 Q_e t} \quad (14)$$

Q_t and Q_e are the adsorption capacities at time t (min) and at equilibrium, respectively, mg·g^{-1}; k_1 and k_2 are the rate constants of the corresponding models, respectively, (min^{-1}), (g mg^{-1}·min^{-1}).

$$\Delta G = -RT \ln K_c \quad (15)$$

$$\ln(K) = -\frac{\Delta H}{R}\frac{1}{T} + \frac{\Delta S}{R} \quad (16)$$

2.5. Techno-Economic Calculation Method

For a single-stage adsorption treatment of oil-contaminated wastewater [24], the required amount of sorbent material m was calculated using Equation (17):

$$m = \frac{Q \cdot (C_0 - C)}{a} \quad (17)$$

The adsorption coefficient k was determined using Equation (18):

$$k = \frac{a}{c_k} \quad (18)$$

For multistage adsorption treatment with sequential addition of the adsorbent into the aqueous phase, the adsorbent dosage for each stage was determined, and the total required amount of sorbent material was calculated using Equation (19):

$$m_1 = \frac{Q}{k}\left(\sqrt[4]{\frac{C_0}{C} - 1}\right) \quad (19)$$

The oil concentration after treatment, C, is determined using the following equation:

$$C = \left(\frac{Q}{Q + k + m_1}\right) \cdot C_0 \quad (20)$$

The number of treatment stages, n, was determined using the following equation:

$$n = \frac{\lg C_0 - \lg C}{\lg(Q + k \cdot m_1) - \lg Q} \quad (21)$$

The total consumption of sorbent material, m_0, was calculated using the following equation:

$$m_0 = n \cdot m_1 \quad (22)$$

m—required mass of sorbent for single-stage treatment (g); k—adsorption coefficient; C_0—initial oil concentration in wastewater (mg·L^{-1}); C—oil concentration after treatment (mg·L^{-1}); n—number of adsorption stages; m_0—total sorbent consumption for multistage treatment (t).

To evaluate the technological feasibility and economic efficiency of the proposed adsorption process, additional calculations were performed to estimate sorbent consumption, treatment cost, and environmental damage reduction.

The annual consumption of adsorbent material, P (kg·year^{-1}), was calculated using the following equation:

$$P = m_c \cdot n \quad (23)$$

m_c—mass of adsorbent required to load a single adsorption filter (kg); n—number of adsorption filters used for wastewater treatment; t_{oper}—annual operating time (h·year^{-1}); Q_1—volumetric flow rate of the liquid (m^3·h^{-1}); C_0—initial concentration of oil in wastewater (g·m^{-3}).

The annual cost of producing the sorption material, Z (thousand USD), was estimated based on the unit price of the adsorbent and its annual consumption according to the following equation:

$$Z = C \cdot P \quad (24)$$

C—cost of the adsorbent (thousand USD·t^{-1}); P—annual consumption of adsorbent material (t·year^{-1}).

The specific cost of water treatment per cubic meter using the adsorbent, $Z_{1\,m3}$ (USD·m^{-3}), was calculated using Equation (25):

$$Z_{1m^3} = \frac{Z}{Q} \quad (25)$$

The quantitative assessment of environmental and economic damage caused by oil and petroleum product contamination of water resources was carried out using a methodology based on a regulatory formula officially approved and recommended by the environmental protection authorities of the Kazakhstan. The economic damage associated with exceeding permissible discharge limits for oil and petroleum products was calculated as follows:

$$D = (C_f - C_{\text{lim}}) \cdot V \cdot K \cdot S \cdot 10 \cdot K_1 \cdot K_2 \quad (26)$$

D—economic damage caused by oil and petroleum product pollution of water resources (USD); C_f—actual concentration of oil and petroleum products in wastewater (mg·L^{-1}); C_{lim}—permissible discharge limit for oil and petroleum products (mg·L^{-1}); V—volume of wastewater discharged during the assessment period (not exceeding 90 days) (million m^3); K—relative hazard coefficient; S—charge rate for the discharge of one conditional ton of pollutants approved by local authorities for the current year (USD·conditional ton^{-1}); 10—penalty factor; K_1—environmental hazard coefficient; K_2—environmental risk coefficient.

3. Results and Discussion

3.1. Adsorption Performance

3.1.1. Equilibrium Adsorption Isotherms and Comparative Performance

The adsorption performance of the prepared materials was evaluated in relation to their specific surface area and pore-volume characteristics (Figure 1). The sorption properties of the investigated natural and composite adsorbents (bentonite, vermiculite, and their mixtures) were assessed using the iodine number and methylene blue adsorption methods [25–29]. The resulting values were compared with literature data for commercial adsorbents, as summarized in Table 1.

Table 1. Comparative characteristics of the adsorption performance of commercial and studied sorbents.

Adsorbent	Specific Surface Area (m^2/g)		Pore Volume (cm^3/g)	Methylene Blue Adsorption (mg·g^{-1})	Iodine Number (mg·g^{-1})	Reference
	Iodine Adsorption	Methylene Blue Adsorption				
Activated carbon (powder)	1056–1452	6000–10000	0.3–1.0	300–500	800–1100	[30,31]
Biochar	50–300	100–400	0.10–0.45	0.10–0.45	0.10–0.45	[32]
Natural zeolite (clinoptilolite)	52.8–132	200–1000	0.1–0.3	10–50	40–100	[33]
Bentonite	7.12 ± 0.02	1500.4 ± 0.02	1.1253	75.02 ± 0.02	5.4 ± 0.01	-
Vermiculite	13.72 ± 0.02	300 ± 0.02	0.225	15.0 ± 0.03	10.4 ± 0.01	-
Bentonite Vermiculite (1:1)	14.78 ± 0.02	600 ± 0.02	0.45	30.00 ± 0.02	11.2 ± 0.01	-
Bentonite Vermiculite (1:2)	21.38 ± 0.02	936.4 ± 0.02	0.7023	46.82 ± 0.02	16.2 ± 0.01	-

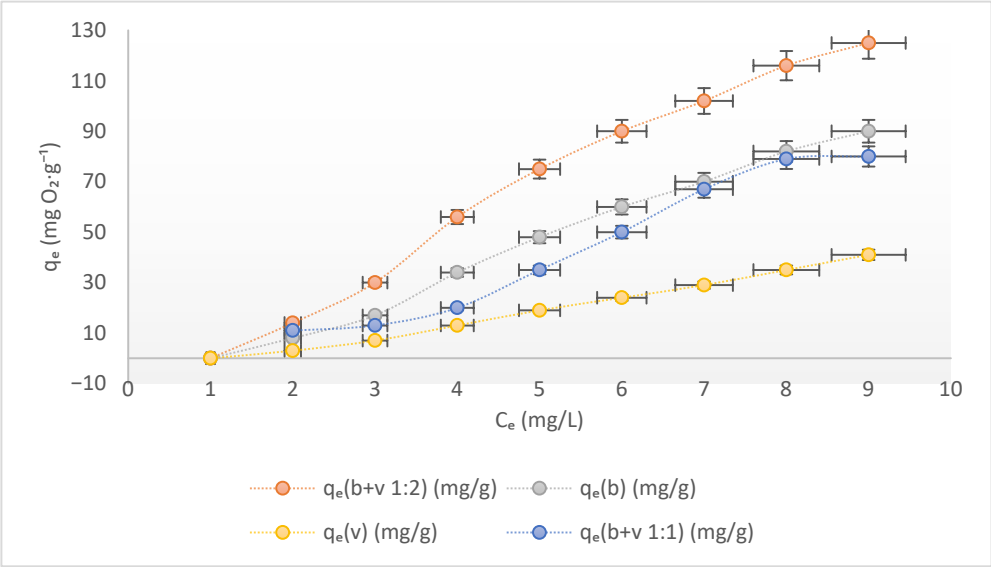

Figure 1. Equilibrium adsorption isotherms showing the dependence of adsorption capacity (q_e, mg·g^{-1}) on the equilibrium adsorbate concentration in solution (C_e, mg·L^{-1}) for mineral sorbents: a bentonite–vermiculite composite (b + v: (1:1) and (1:2), pure bentonite (b), and vermiculite (v).

The equilibrium adsorption capacity (q_e, mg g^{-1}) was calculated using Equation (1), following the procedure reported in [10,25].

All curves display a shape commonly associated with predominantly physical adsorption: as the adsorbate concentration increases, the incremental rise in q_e progressively diminishes and the isotherms approach a plateau. This behavior reflects gradual occupation of available sorption sites and the finite maximum uptake for each sorbent.

Among the tested sorbents, the bentonite–vermiculite composite exhibits the highest adsorption capacity across the entire concentration range. Its isotherm shows a steep increase at low C_e followed by a more gradual approach to saturation at higher concentrations, which is consistent with a heterogeneous surface featuring sites of different affinities and suggests a beneficial interaction between the composite components. In particular, the high surface activity of bentonite combined with the developed pore structure of vermiculite likely enhances the overall uptake, enabling efficient removal even at low contaminant concentrations.

Bentonite shows an intermediate performance: q_e increases more gradually than for the 1:2 composite and reaches a lower maximum value, which may be attributed to a lower specific surface area and a narrower distribution of effective adsorption sites.

The adsorption isotherm of vermiculite (v) exhibits the lowest adsorption capacity among the investigated materials, which is evidenced by the smallest slope of the isotherm over the studied concentration range. The uptake is governed primarily by physisorption on the external surface and within the pore structure and may additionally involve surface precipitation of residual metal oxide species. The adsorption isotherm of the bentonite–vermiculite composite (1:1) coincides with that of the 1:2 composite at the initial stage of adsorption; however, at higher loadings its uptake decreases, which can be attributed to progressive surface deactivation of the sorbent.

Overall, the isotherms demonstrate that the bentonite–vermiculite (1:2) composite is the most efficient sorbent for removing organic contaminants from aqueous media. Its superior performance results from a combination of multiple adsorption mechanisms, well-developed porosity, and high surface reactivity. The use of such composite mineral sorbents provides a substantial improvement in purification efficiency compared with the application of individual minerals [26–29].

The comparative analysis indicates that the bentonite–vermiculite composite (1:2) exhibits the most balanced and promising overall properties, with a specific surface area of 936.4 m^2/g (MB-based) and a pore volume of 0.7023 cm^3/g, which are comparable to those of activated carbon (800–1500 m^2/g; 0.3–1.0 cm^3/g) [30–34]. Although the iodine adsorption capacity is relatively low (21.38 m^2/g), the high methylene blue uptake suggests a predominance of mesopores, which are particularly effective for the adsorption of relatively large organic molecules, including petroleum hydrocarbons and dye compounds. In contrast, biochar typically exhibits lower surface areas (50–300 m^2/g) and MB adsorption capacities (10–45 $mg \cdot g^{-1}$), consistent with a less developed porous structure [35]. Overall, the composite shows adsorption characteristics superior to biochar and approaching those of activated carbon, while remaining more accessible and environmentally benign. These results are also consistent with literature reports that composite sorbents often outperform single-component materials in the removal of petroleum pollutants from water [36].

3.1.2. Effect of Contact Time on Adsorption Capacity

The effect of contact time on the adsorption capacity of bentonite and the bentonite–vermiculite composite was investigated to evaluate the adsorption kinetics and determine the time required to reach equilibrium (Figure 2). For both sorbents, the adsorption capacity increased rapidly during the initial stage of the process, followed by a gradual decrease in the adsorption rate until equilibrium was attained.

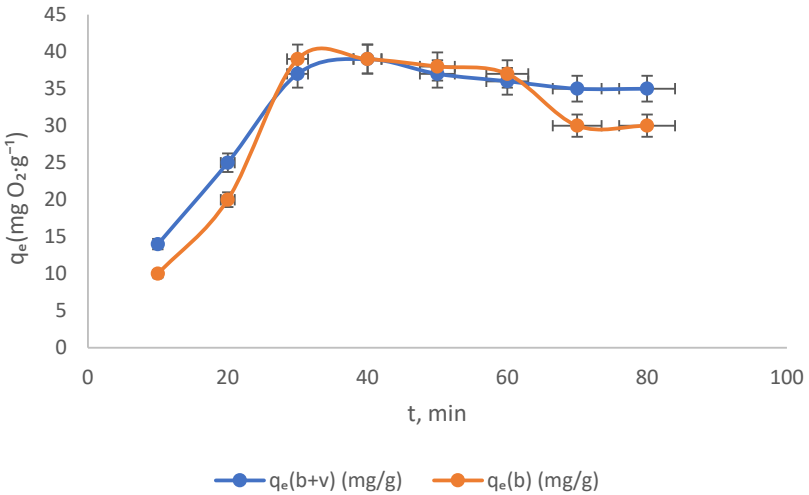

Figure 2. Effect of contact time on adsorption capacity of bentonite and bentonite–vermiculite composite.

The fast uptake observed within the first 20–30 min can be attributed to the availability of a large number of vacant active sites on the sorbent surface, enabling rapid adsorption driven by surface diffusion and external mass transfer. As adsorption proceeds, the number of accessible sorption sites decreases, leading to a slower increase in adsorption capacity due to progressive site saturation and diffusion limitations within the pore structure.

The bentonite–vermiculite composite exhibits a higher adsorption capacity throughout the entire contact time range compared to pure bentonite. This behavior indicates a synergistic effect between bentonite and vermiculite, resulting from the combination of layered clay minerals and expanded porous structures, which facilitates both surface adsorption and intraparticle diffusion. Similar kinetic trends have been reported for composite mineral sorbents used for the removal of petroleum hydrocarbons and organic dyes, where equilibrium is typically achieved within 30–60 min under batch conditions [37,38].

The attainment of adsorption equilibrium within a relatively short contact time demonstrates the practical applicability of the proposed composite sorbent for wastewater treatment, as reduced residence times are advantageous for industrial-scale processes.

3.1.3. Effect of pH on Adsorption Capacity

The influence of solution pH on the adsorption capacity of bentonite and the bentonite–vermiculite composite was examined over a wide pH range to assess the role of surface charge and adsorbate–adsorbent interactions (Figure 3). The adsorption capacity of both materials shows a pronounced dependence on pH, with a noticeable increase in adsorption efficiency from acidic to near-neutral conditions.

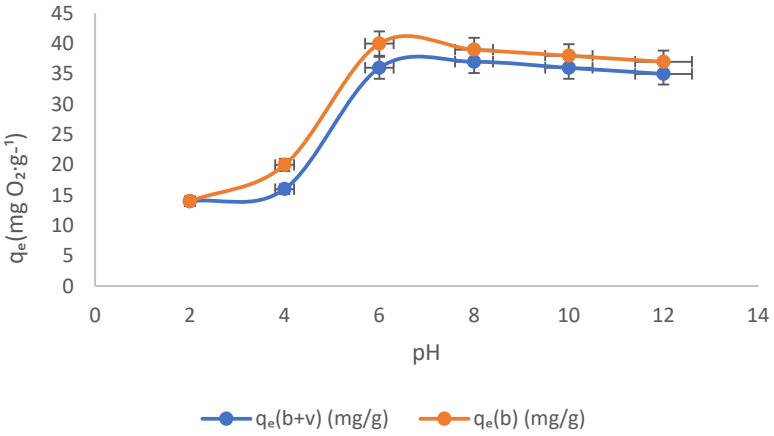

Figure 3. Influence of pH on the adsorption performance of mineral sorbents.

At low pH values, adsorption is suppressed due to competition between hydrogen ions (H^+) and organic molecules for active sorption sites, as well as partial protonation of surface functional groups, which reduces electrostatic attraction. As the pH increases to near-neutral values (pH 6–8), adsorption capacity reaches a maximum, indicating favorable electrostatic interactions and enhanced accessibility of adsorption sites.

At higher pH values, the adsorption capacity tends to stabilize or slightly decrease, which may be associated with increased electrostatic repulsion between negatively charged sorbent surfaces and dissociated organic species, as well as possible changes in the aggregation state of oil-derived compounds. The bentonite–vermiculite composite consistently exhibits higher adsorption capacities across the entire pH range, confirming its enhanced surface reactivity and buffering capacity compared to individual minerals.

These observations are consistent with previous studies reporting that clay-based and composite sorbents exhibit optimal adsorption performance in neutral or slightly alkaline environments when treating oil-contaminated waters and organic pollutants [38]. The broad pH tolerance of the composite sorbent highlights its suitability for real wastewater systems, where pH conditions can vary significantly.

3.1.4. Effect of Sorbent Dose on Equilibrium Adsorption Capacity (q_e)

To evaluate the effect of sorbent dosage on the adsorption of an oil-in-water emulsion, sorbent masses in the range of 0.50–0.95 g were tested while maintaining pH at 6.86; all experiments were performed at 25 °C with a contact time of 30 min and an initial oil concentration of 100 ppm, the suspension was agitated using a magnetic stirrer at 150 rpm, and the adsorption progress was monitored by measuring the residual concentration via chemical oxygen demand (COD) at 10 min intervals; the results are presented in Figure 4 as the dependence of the equilibrium adsorption capacity, q_e (mg·g^{-1}), on sorbent mass.

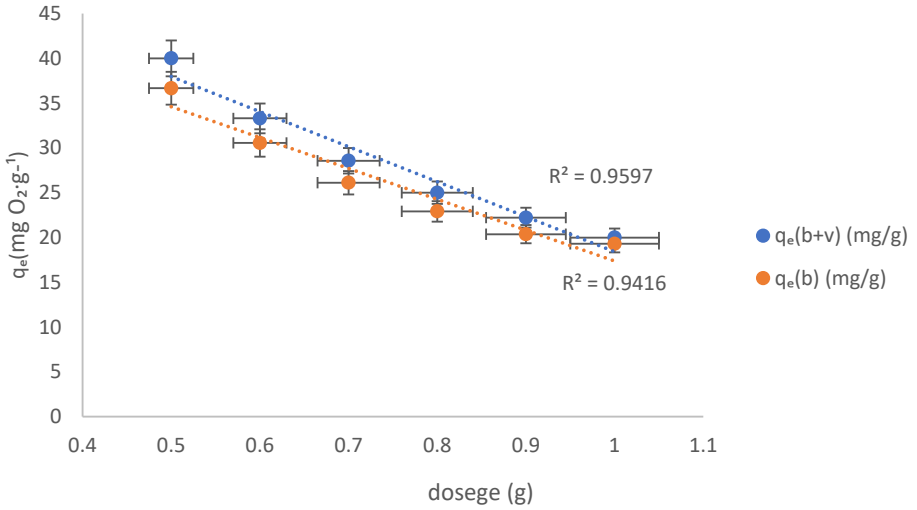

Figure 4. Effect of sorbent dose on adsorption capacity (q_e) for determining the optimal sorbent mass during oil removal from water: bentonite–vermiculite composite (b + v) and bentonite (b).

Figure 4 shows that increasing the sorbent dose from 0.5 to 1.0 g leads to a monotonic decrease in the equilibrium adsorption capacity q_e (mg·g^{-1}) for both the bentonite–vermiculite composite (b + v) and pristine bentonite (b). Within the investigated range, the data are well represented by linear trendlines ($R^2 \approx 0.96$ for b + v and $R^2 \approx 0.94$ for b), indicating a robust and reproducible dose effect under the selected experimental conditions. The observed decline in q_e with increasing sorbent mass is typical for systems operated at a fixed initial pollutant loading and can be attributed to the redistribution of a finite sorbate amount over a larger sorbent mass "capacity dilution", as well as to partial masking of accessible surface sites and mass-transfer limitations promoted by particle aggregation at higher dosages.

A comparative assessment further demonstrates that the composite (b + v) consistently outperforms bentonite in terms of q_e across the entire dose interval: the difference is more pronounced at low dosages (0.5–0.7 g), whereas the curves converge as the dose approaches 1.0 g, suggesting that the relative contribution of the composite's structural advantages becomes less significant under sorbent-excess conditions. The higher q_e values for b + v are plausibly associated with the incorporation of vermiculite, which increases the fraction of readily accessible oil-binding sites through a more developed pore architecture (including mesoporosity), thereby enhancing hydrocarbon retention and reducing the propensity for secondary release under mechanical agitation. These findings are consistent with previous reports on vermiculite-based (including modified) sorbents for oil-contaminated water treatment, which highlight high oil affinity and a strong dependence of retention performance on oil concentration and modification route [10,21].

At higher sorbent dosages, particle aggregation and bed compaction become more likely, which may partially block accessible active sites, reduce the effective interfacial area, and deteriorate mass transfer in the suspension (localized diffusion limitations, increased viscosity, and restricted access to the pore network). Consistent trends have been reported in the adsorption-based treatment of oil-contaminated waters, where increasing the sorbent mass typically enhances the overall removal efficiency but is accompanied by a decrease in the specific adsorption capacity; for bentonite-driven oil-emulsion treatment systems, in particular, sorbent dosage has been shown to markedly affect both extraction performance and the equilibrium characteristics of the oil phase [2,22].

3.2. Structure and Surface Characterization

3.2.1. Surface Morphology and Elemental Composition (SEM/EDS)

The crystalline structure of bentonite is governed by a layered TOT-type architecture, in which a central octahedral sheet composed of aluminum and/or magnesium oxides is sandwiched between two external tetrahedral silica sheets; the oxygen ions of the octahedral layer are oriented toward the tetrahedral [38–40]. Surface hydroxyl groups of the clay packets act as reactive sites, which determines their importance for targeted functionalization and chemical modification of sorbent surfaces [41].

The influence of mineral composition on adsorption performance during the removal of petroleum products from aqueous media was evaluated through an integrated analysis of both the solid and liquid phases of the studied samples.

According to spectroscopic and microscopic analyses, the investigated bentonite sample is a finely dispersed Na-montmorillonite with a dominant aluminosilicate TOT structure (T = Si, Al), in good agreement with previously reported [42]. A high oxygen content (51.73 wt.%) together with substantial amounts of silicon (17.04 wt.%) and aluminum (7.76 wt.%) confirms the phyllosilicate nature of the material (Figure 5a).

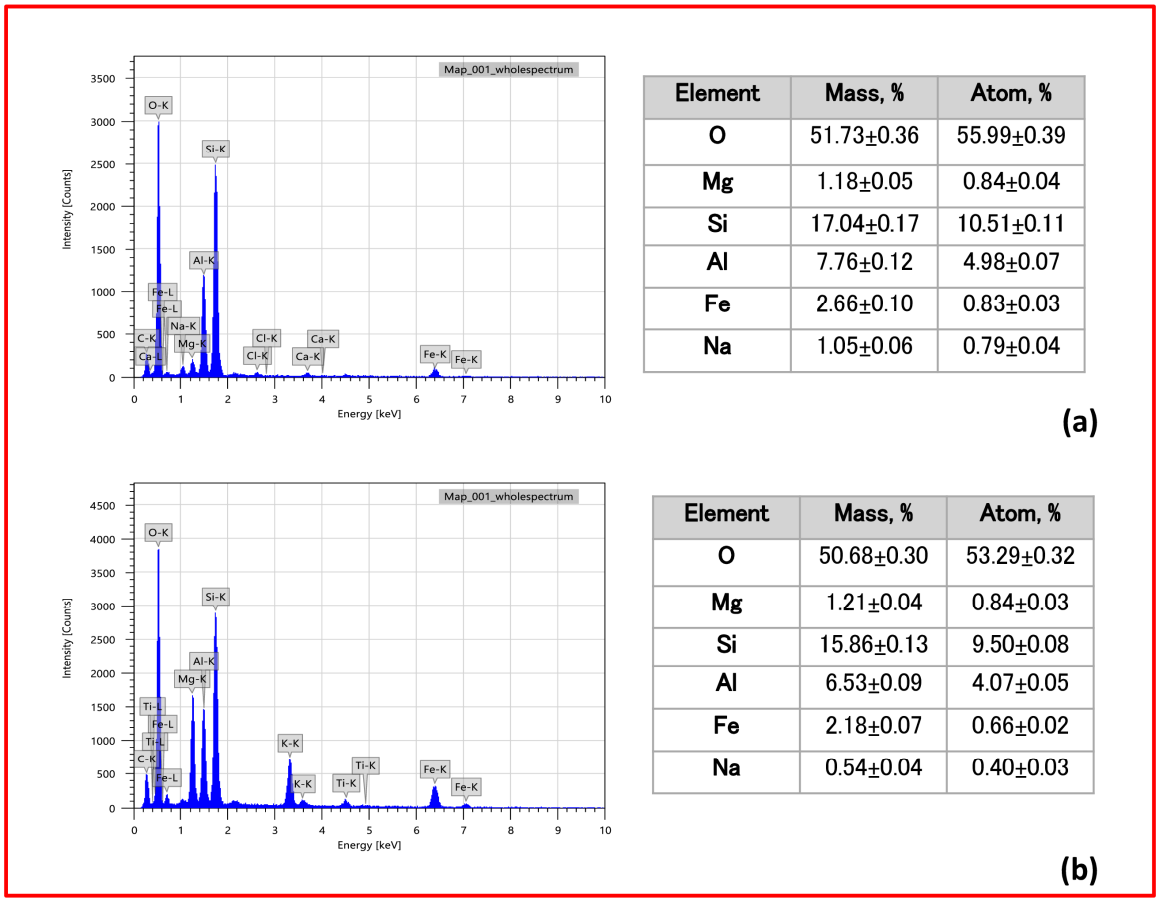

Element	Mass, %	Atom, %
O	51.73±0.36	55.99±0.39
Mg	1.18±0.05	0.84±0.04
Si	17.04±0.17	10.51±0.11
Al	7.76±0.12	4.98±0.07
Fe	2.66±0.10	0.83±0.03
Na	1.05±0.06	0.79±0.04

Element	Mass, %	Atom, %
O	50.68±0.30	53.29±0.32
Mg	1.21±0.04	0.84±0.03
Si	15.86±0.13	9.50±0.08
Al	6.53±0.09	4.07±0.05
Fe	2.18±0.07	0.66±0.02
Na	0.54±0.04	0.40±0.03

Figure 5. Energy-dispersive X-ray spectroscopy (EDS) analysis of bentonite: (**a**) pristine sample (before sorption); (**b**) bentonite after sorption.

The cation-exchange behavior and the occurrence of isomorphous substitutions are governed by the presence of minor components: Na (1.05 wt.%), Mg (1.18 wt.%) and Fe (2.66 wt.%). These elements reflect substitution mechanisms typical for montmorillonites ($Mg^{2+} \rightarrow Al^{3+}$ in octahedral sites; $Fe^{3+}/Fe^{2+} \rightarrow Al^{3+}$ in tetrahedral positions), leading to the development of an excess negative charge within the TOT layers. Charge compensation is achieved by interlayer Na^{+} and Mg^{2+} cations, which ensures a high cation-exchange

capacity and, consequently, a pronounced ability of bentonite to bind polar components of hydrocarbon mixtures via ion-exchange and dipole-ion interactions [5,43].

SEM micrographs of pristine bentonite reveal a well-developed submicron porosity formed by randomly oriented platy particles, which provides a high specific surface area and facilitates access to interlayer channels that are essential for the adsorption of organic compounds. The presence of dispersed amorphous domains is observed in the micrographs as light gray regions (Figure 5a). According to EDS mapping, Si, Al, and O are uniformly distributed, confirming the homogeneous aluminosilicate nature of montmorillonite, whereas local enrichments in Na, Mg, and Fe may be associated with minor inclusions that form additional active sites. The atomic fractions of O (65.53 at.%), Si (12.71 at.%), and Al (4.70 at.%) correspond to the composition of dioctahedral montmorillonite [38]. Traces of K and Ti observed in the EDS spectrum are attributed to secondary contamination introduced during drilling operations, where metallic components of drilling equipment may contribute minor elemental inputs to the aquatic environment. Due to their very low concentrations, these elements do not significantly affect the sorption properties of the studied material (Figure 5b).

The investigation of the bentonite–vermiculite (1:2) composite revealed an "expanded" aluminosilicate oxide profile with the following hierarchy: SiO_2 > Al_2O_3 > (MgO + Fe_2O_3 + Na_2O) (+TiO_2) (Figure 6b–d). The increased intensity of the Mg and Fe signals compared to Na-bentonite confirms the contribution of vermiculite, while the weak Ti signal indicates the presence of natural titanium-containing phases [5,44].

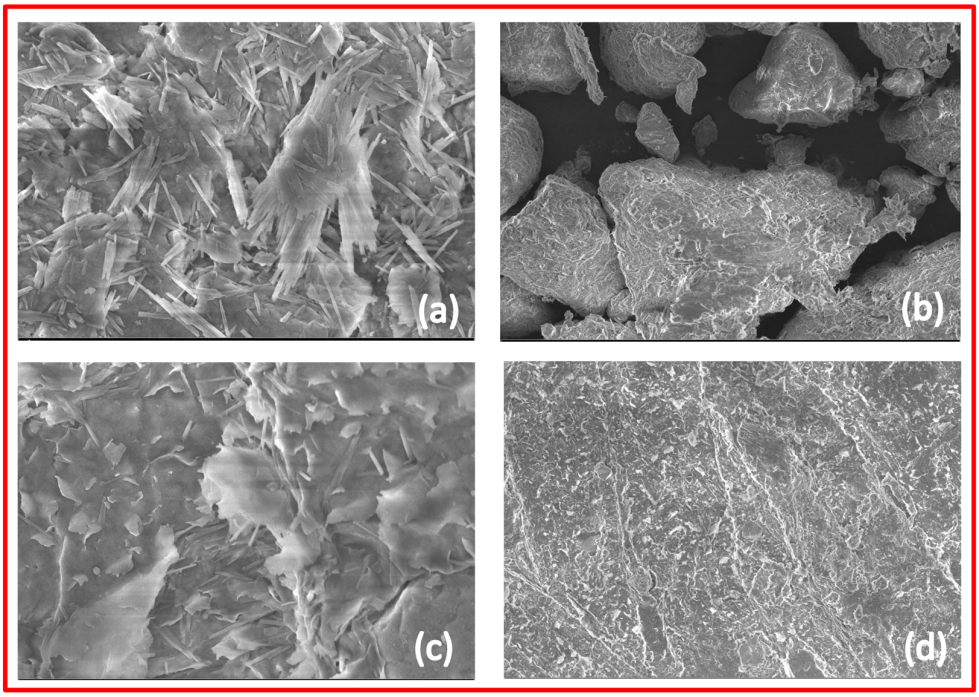

Figure 6. SEM micrographs of bentonite-based sorbents: (**a**,**b**) bentonite before adsorption and (**c**,**d**) after adsorption of oil-contaminated water.

Elemental mapping (Figure 7b) demonstrates a mosaic structural organization: Si, Al, and O constitute the primary matrix; Mg- and K-rich regions correspond to vermiculite-enrich domains, and localized Fe and Ti clusters may form as potential Lewis acid sites. SEM analysis (Figure 8a,b) reveals a distinct two-phase morphology, where dense montmorillonite aggregates coexist with lamellar vermiculite domains. This structural arrangement forms slit-like pores and microcracks, providing an efficient surface for mass transfer.

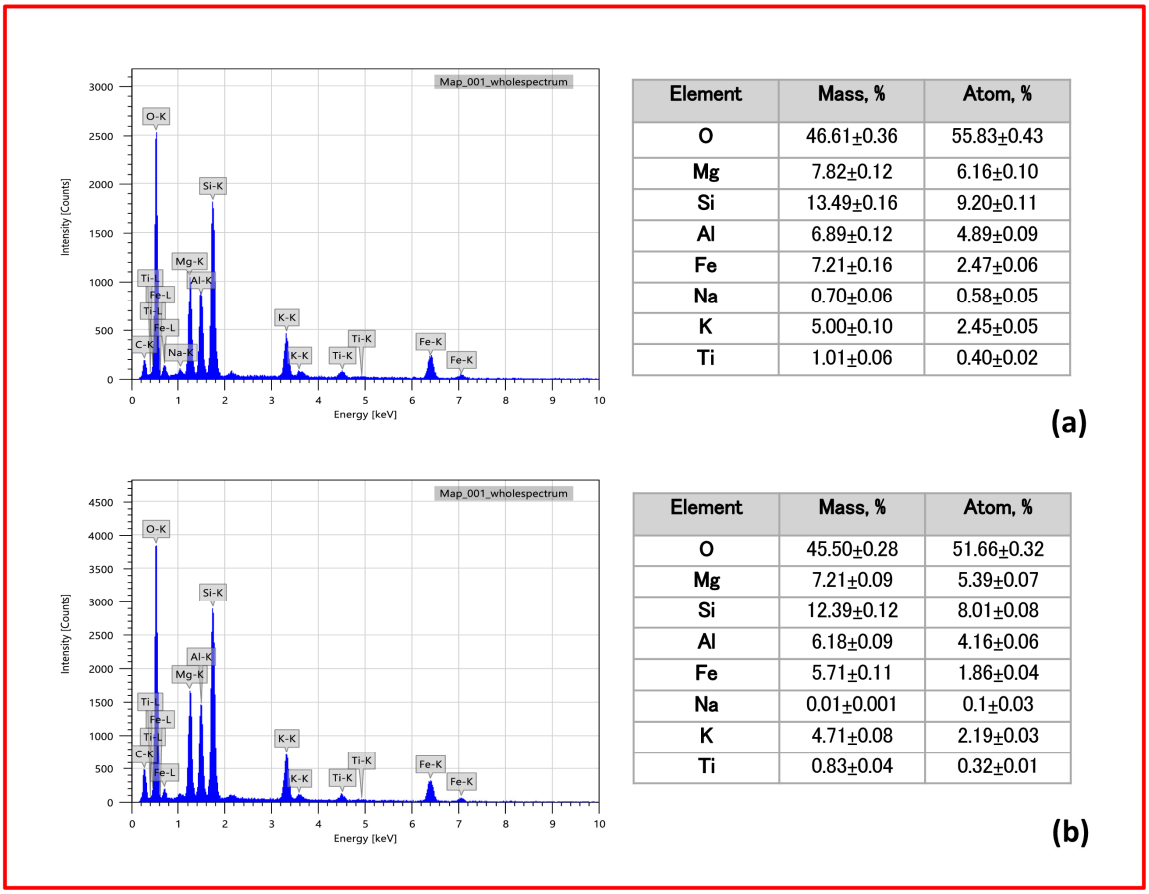

Element	Mass, %	Atom, %
O	46.61±0.36	55.83±0.43
Mg	7.82±0.12	6.16±0.10
Si	13.49±0.16	9.20±0.11
Al	6.89±0.12	4.89±0.09
Fe	7.21±0.16	2.47±0.06
Na	0.70±0.06	0.58±0.05
K	5.00±0.10	2.45±0.05
Ti	1.01±0.06	0.40±0.02

Element	Mass, %	Atom, %
O	45.50±0.28	51.66±0.32
Mg	7.21±0.09	5.39±0.07
Si	12.39±0.12	8.01±0.08
Al	6.18±0.09	4.16±0.06
Fe	5.71±0.11	1.86±0.04
Na	0.01±0.001	0.1±0.03
K	4.71±0.08	2.19±0.03
Ti	0.83±0.04	0.32±0.01

Figure 7. Energy-dispersive X-ray spectroscopy (EDS) analysis of the bentonite–vermiculite (1:2) composite: (**a**) pristine sample (before sorption); (**b**) composite after sorption.

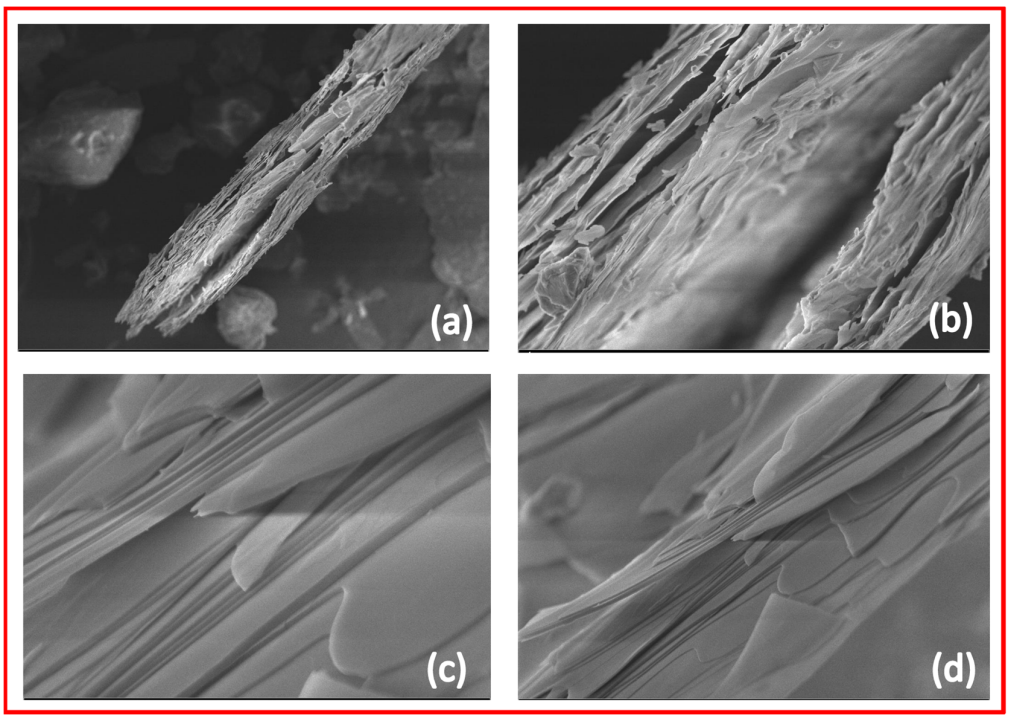

Figure 8. SEM micrographs of the bentonite–vermiculite (1:2) composite before sorption: (**a**,**b**) before adsorption and (**c**,**d**) after adsorption of oil-contaminated water.

The higher intensities of the Mg and Fe signals relative to Na-bentonite confirm the contribution of vermiculite, whereas the weak Ti signal can be attributed to the presence of naturally occurring Ti-bearing phases [45].

According to quantitative EDS data, the combined content of SiO_2 and Al_2O_3 accounts for approximately 60 wt.%, whereas the contents of MgO and Fe_2O_3 are each on the order of ~7 wt.%. The Na_2O content decreases to below 1 wt.%, while TiO_2 is detected at a level of 1–1.5 wt.%. An Mg/Na ratio greater than 7 reflects partial substitution of interlayer Na^+ by Mg^{2+} and the formation of a mixed Na^+/Mg^{2+} cation-exchange system. Overall, the incorporation of vermiculite transforms the initial Na-bentonite into a more functional sorbent combining ion-exchange and acidic sites, which is consistent with literature reports on the enhanced performance of such composite materials [46].

The stability of the positions of the main diffraction maxima (shift < 0.05°) and the preservation of the complete set of characteristic reflections indicate retention of the mixed-layer nature of the composite and the absence of phase transformations (in particular, of the "vermiculite → smectite" type). Overall, adsorption of petroleum products is accompanied by partial loosening and dispersion of the structure with increased microdefect density, while simultaneously promoting the formation of a more ordered packet arrangement. This combination of increased effective surface area (due to fragmentation) and enhanced mechanical stability (due to layer compaction and rearrangement) substantiates the high potential of the composite for repeated use in cyclic wastewater treatment processes [45].

3.2.2. Crystal Structure and Phase Composition (XRD)

To quantify sorbent structural transformations arising from interactions with petroleum-derived species, lattice characteristics were evaluated using X-ray diffraction data. The XRD patterns (10–90° 2θ°) of pristine bentonite (b (pure)) and the bentonite–vermiculite composite (b + v (pure)) confirm the preservation of the layered aluminosilicate framework and the successful contribution of the vermiculite phase in the composite (Figure 9). For b (pure), the diffractogram is dominated by reflections typical of bentonite-rich clays, with a pronounced peak near $2\theta^\circ \approx 26.6^\circ$ attributable to quartz and a set of moderate-intensity features in the ~19–37° region associated with the clay mineral matrix and common accessory phases. Compared with b (pure), b + v (pure) exhibits a denser set of reflections and a noticeable enhancement of peaks in the ~24–37° range, alongside more distinct high-angle features in the ~50–62° window (including an intensified contribution around ~58–60° 2θ°), consistent with the expected diffraction signature of vermiculite in layered mineral assemblages; these changes support that vermiculite provides additional ordered silicate domains superimposed on the bentonite background. After petroleum uptake, b + v (after) retains the main peak positions observed for b + v (pure), indicating that no new crystalline phases form and that the mineral skeleton remains structurally stable under sorption conditions; however, the pattern shows a systematic increase in the diffuse background (most evident across ~20–35°) and a redistribution of relative peak intensities within the highlighted regions. Such behavior is consistent with partial surface coverage and pore/interlayer filling by an X-ray–amorphous organic fraction (hydrocarbon film), which elevates the scattering baseline and attenuates certain reflections without shifting their 2θ° positions. Notably, because the present scan starts at 10° 2θ°, the basal (001) reflections of vermiculite at low angles are not captured; therefore, the XRD discussion here emphasizes framework stability and phase contributions rather than direct quantification of interlayer expansion.

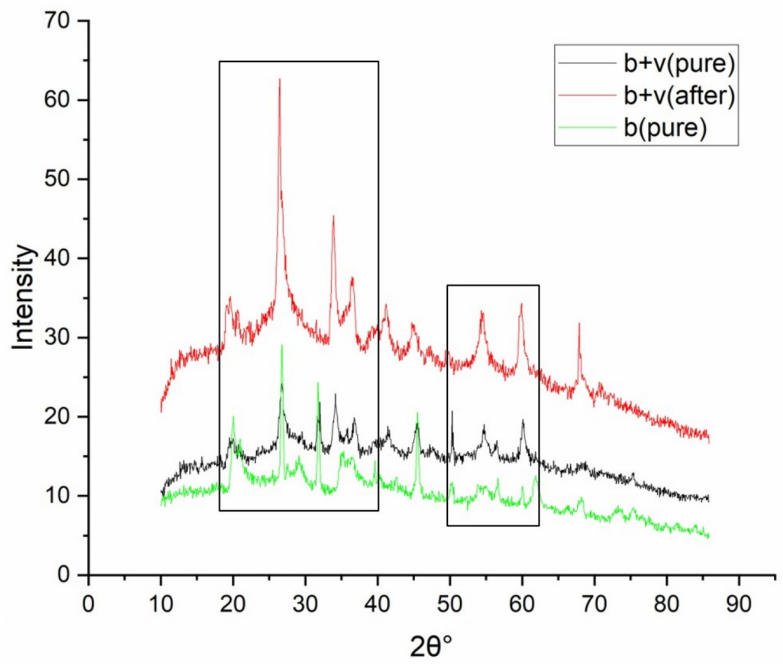

Figure 9. XRD patterns of the bentonite–vermiculite composite mixture before and after sorption.

The phase-level interpretation of the present patterns is consistent with prior XRD-based analyses of bentonite-containing composites (Table 2). In particular, Li et al. showed that the characteristic reflections of bentonite (including quartz and montmorillonite contributions) are retained after processing and remain discernible after loading an organic phase, supporting the view that the mineral framework is preserved while the guest phase is incorporated primarily through physical confinement/interaction rather than the formation of new crystalline products [47–49]. In the present study, the retention of the principal peak positions from b + v (pure) to b + v (after), accompanied by an increased diffuse background and a redistribution of relative peak intensities, is consistent with behavior commonly reported for mineral–organic composite systems. Specifically, the sorbed organic fraction is expected to contribute predominantly X-ray–amorphous scattering and to partially attenuate selected reflections through surface coverage and filling of pores and interlayer spaces, while leaving the underlying mineral peak positions essentially unchanged [47]. A similar approach is also adopted in recent oil-sorption designs that incorporate bentonite into hydrophobic composite sponges (e.g., PDMS/ZIF-8/bentonite), where XRD is used to verify that bentonite retains its characteristic reflections in the composite and thus serves as a structurally robust mineral component within the multifunctional sorbent architecture [48].

Table 2. XRD-derived structural parameters of bentonite and bentonite–vermiculite composite before and after sorption.

Sample	Crystallite Size (Scherrer), Å	Crystallite Size (W–H), Å	Lattice Microstrain (ε)	Crystallinity, %
b initial	792.88482	488.86618	0.00015	44.74884
b + v before	915.72601	530.20084	0.00032	45.03035
b + v after	1294.53314	607.70830	−0.00040	32.21380

Collectively, these comparisons support that the mineral skeleton in b and b + v remains intact under the employed conditions, whereas the post-sorption changes for b + v (after) are best attributed to the presence of an X-ray–amorphous hydrocarbon fraction and altered scattering at the mineral–organic interface rather than to mineralogical phase transformation.

3.3. Electrokinetic and Colloidal Behavior

At the work [16] showed that cation-exchange reactions within the vermiculite structure are a key factor governing its wettability, allowing the surface to shift from superhydrophilic behavior toward a more hydrophobic state. This result suggests that introducing vermiculite into a bentonite matrix may tune the composite sorbent's surface characteristics by decreasing overall hydrophilicity and strengthening hydrophobic interfacial interactions.

To substantiate this effect more rigorously, it is advisable to evaluate the location of the slipping plane within the electrical double layer of colloidal systems, which can be assessed through measurement and interpretation of ζ-potential values [16].

As reported in several studies [13,19], variations in pH exert only a minor influence on the ζ-potential of both bentonite and its mixture with vermiculite. Bentonite particles in aqueous media were shown to exhibit no isoelectric point and to maintain a negative ζ-potential across the entire pH range of 2–12 [20,21], in agreement with previous findings [21]. The electrokinetic parameters of the pristine and sorption-loaded samples are summarized in Table 3. Under the measurement conditions (pH 6.86, 1 mM KCl, 25 °C), the pristine bentonite and the bentonite–vermiculite composite exhibited comparably high negative ζ-potentials (−37.0 and −38.6 mV, respectively), indicating well-developed negative surface charge and electrostatic stabilization of the suspensions. The electrophoretic mobility followed the same trend, which is consistent with the Smoluchowski relationship (μ∝ζ) for aqueous dispersions. According to Table 3, sorption from oil-contaminated water induces distinct changes in the electrical surface charge characteristics of the investigated minerals.

Table 3. Electrokinetic parameters of bentonite–vermiculite (1:2) and bentonite suspensions before and after sorption (KCl background; I = 25.9–26.8 mM, pH 6.0, 25 °C): ⟨ζ⟩, ⟨μ⟩, D, and σ.

Sample	Condition	⟨ζ⟩, mV	⟨μ⟩, (μm s^{-1})/(V cm^{-1})	D, 10^{-10} m^2 s^{-1}	σ, mC m^{-2}
Bentonite–Vermiculite	pure	−38.6 ± 1.1	−3.01 ± 0.09	7.74 ± 0.23	−15.6
	after sorption	−23.3 ± 2.7	−1.82 ± 0.20	4.67 ± 0.51	−8.9
Bentonite	pure	−37.0 ± 1.4	−2.89 ± 0.11	7.43 ± 0.28	−15.1
	after sorption	−35.9 ± 2.9	−2.80 ± 0.27	7.20 ± 0.69	−14.3

A markedly different behavior was observed after sorption. For vermiculite–bentonite, sorption led to a pronounced decrease in the absolute ζ-potential from −38.6 to −23.3 mV, accompanied by a decrease in |μ| (−3.01 to −1.82) and a substantial reduction in the magnitude of surface charge density σ (−15.6 to −8.9 mC·m^{-2}) (Table 3). This pattern indicates partial charge neutralization and strong electrostatic screening induced by surface coverage with the sorbed phase and redistribution of counter-ions in the interfacial region. In contrast, bentonite remained largely electrokinetically stable after sorption: ζ-potential and σ changed only slightly (−37.0 to −35.9 mV; −15.1 to −14.3 mC·m^{-2}), suggesting that the net negative surface charge was preserved and that the electrical double layer remained sufficiently repulsive to prevent major destabilization (Table 3). After sorption, the ζ-potential shifts toward less negative values (≈−20 mV), which can be rationalized by partial replacement of interlayer Na^+/K^+ with protonated organic cations and by shielding of negatively charged surface sites through adsorption of Fe- and Ti-containing colloids. Despite this attenuation, ζ remains below −15 mV, implying that the dispersion retains a non-negligible electrostatic repulsion and therefore does not fully lose colloidal stability [16–21].

To connect charge-state changes with hydrodynamic restructuring, the diffusion-based hydrodynamic radius R_h was calculated using the Stokes-Einstein relation, revealing a clear divergence between the samples. Bentonite–vermiculite exhibited strong hydrodynamic growth after sorption (D: 7.74 × 10^{-12} → 4.67 × 10^{-12} m^2·s^{-1}; R_h: 31.7 → 52.5 nm;

$D_h \approx 63 \rightarrow 105$ nm), consistent with formation of an adsorbed layer and/or aggregation driven by reduced electrostatic repulsion at lower $|\zeta|$. By contrast, bentonite showed only a minor change in R_h (33.0 → 34.1 nm), supporting the conclusion that sorption did not substantially destabilize the suspension. This interpretation is further reinforced by the DLS intensity-weighted particle size distributions: because intensity weighting strongly overemphasizes larger particles, the appearance or amplification of micrometer-scale modes indicates the presence of even a small fraction of large agglomerates. This behavior is mechanistically consistent with the pronounced post-sorption attenuation of surface charge and the increase in hydrodynamic diameter of the bentonite–vermiculite composite, as well as with heteroaggregation between vermiculite- and bentonite-derived platelets. Finally, the electrostatic context can be rationalized using Dukhin analysis. Using the effective ionic strength derived from conductivity ($I_{eff} \approx 26$ mM), the Debye length shortens to $\lambda_D \approx 1.88$nm, giving $\kappa_a \approx 5.3 \times 10^2$ for a = 1 μm and small Dukhin numbers (Du ~ 10^{-3}), with a pronounced reduction for bentonite–vermiculite after sorption (0.00259 → 0.00126) but only minor change for bentonite (0.00241 → 0.00233) (Table 4).

Table 4. Debye length and Dukhin parameters for bentonite and bentonite–vermiculite composite (1:2) suspensions before and after sorption (effective ionic strength; KCl background), including reduced Dukhin number (Du *) and Du calculated for a = 1 μm.

Sample	Condition	λ_D, nm	Du *	κa (=a/λ_D)	Du
Vermiculite-Bentonite	pure	1.88	1.376	531.9	0.00259
	after sorption	1.88	0.669	531.9	0.00126
Bentonite	pure	1.86	1.293	537.6	0.00241
	after sorption	1.89	1.233	529.1	0.00233

Reporting both nominal (1 mM KCl; $\lambda_D \approx 1.9$nm) and effective Dukhin parameters is therefore essential: while the nominal values enable standardized comparison to the background electrolyte, the effective values capture the real screening environment created by ion exchange and dissolved species in clay suspensions, and thus better explain why bentonite–vermiculite undergoes charge-driven destabilization and hydrodynamic growth during oil sorption, whereas bentonite maintains interfacial charge and colloidal stability.

3.4. Adsorption Kinethics Investigation

To gain further insight into the adsorption mechanism, kinetic modeling was performed based on the equilibrium concentration data [49]. The experimental results were evaluated using both the pseudo-first-order (PFO) and pseudo-second-order (PSO) kinetic models, and the corresponding fitting curves are presented in Figure 10.

The sorption kinetics of petroleum products on bentonite and on the bentonite–vermiculite mixture were examined using the PFO and PSO models at 293, 303, and 313 K. The corresponding linearized kinetic plots are presented in Figure 10a,b, while the derived rate constants are summarized in Table 5. For bentonite, the PFO model (Figure 10a) shows satisfactory linearity over the entire contact-time range, as evidenced by high determination coefficients ($R^2 \approx 0.9$). The PFO rate constants decrease with increasing temperature, indicating a reduction in the apparent sorption rate upon heating. This trend may be attributed to the weakening of physical interactions between petroleum molecules and the surface active sites of bentonite, as well as partial disruption of weakly bound adsorption complexes at elevated temperatures. In contrast, the PSO model for bentonite (Figure 10b) exhibits less pronounced linearity than the PFO model, particularly at 303 and 313 K, suggesting that sorption on bentonite is governed predominantly by physical adsorption and diffusion-controlled processes rather than by chemisorption implied

by the PSO formalism. For the bentonite–vermiculite mixture, the kinetic behavior differs markedly. As shown in Figure 10b, the PSO model provides higher R^2 values than the PFO model, especially at higher temperatures, indicating that vermiculite incorporation alters the sorption mechanism by enhancing the contribution of adsorption at active sites and interlayer interactions. The PSO rate constants for the bentonite–vermiculite mixture (Table 5) are generally higher than those of pristine bentonite, confirming an overall acceleration of the sorption process. This enhancement can be ascribed to the well-developed layered structure of vermiculite, an increased specific surface area, and the emergence of additional binding sites that facilitate stronger interactions with petroleum fractions. Overall, the comparative kinetic analysis demonstrates that petroleum product sorption on bentonite is better described by the PFO model, whereas the PSO model is more appropriate for the bentonite–vermiculite mixture. These findings confirm that vermiculite incorporation not only increases sorption capacity but also modifies the kinetic mechanism of sorption.

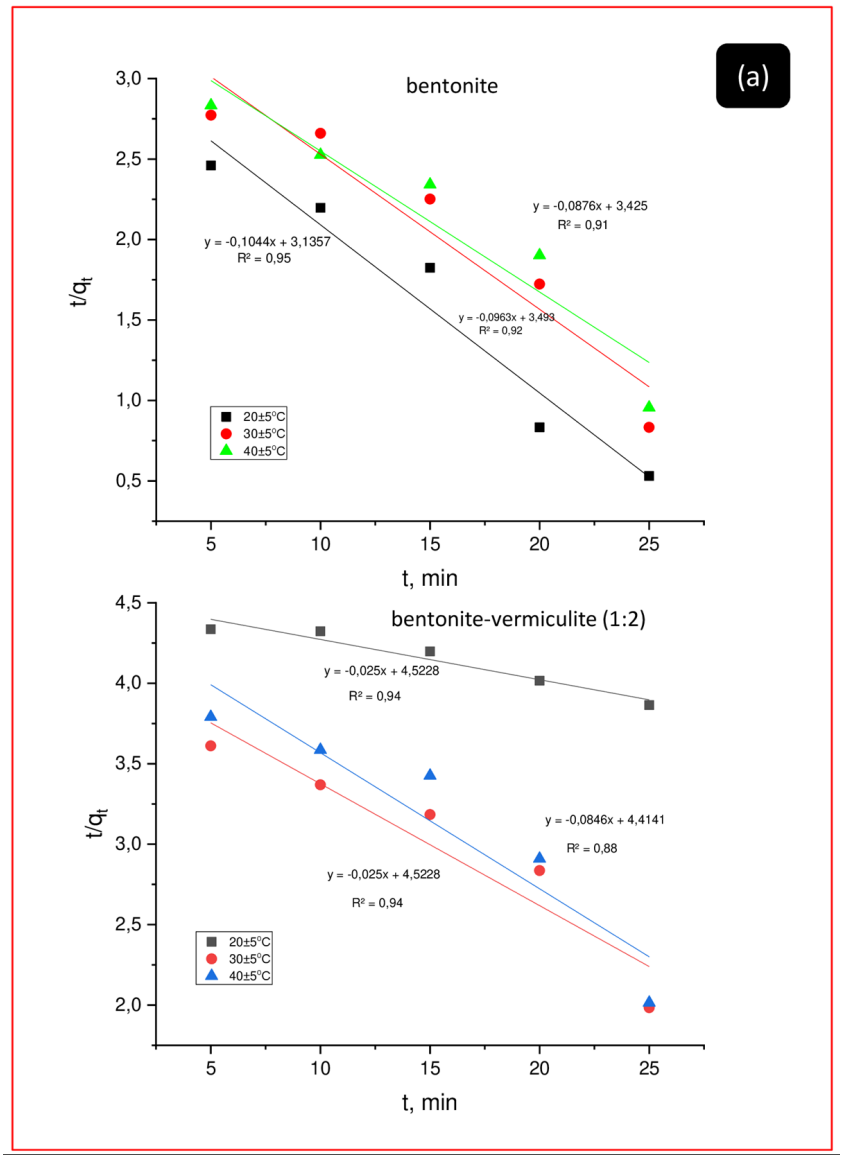

Figure 10. *Cont.*

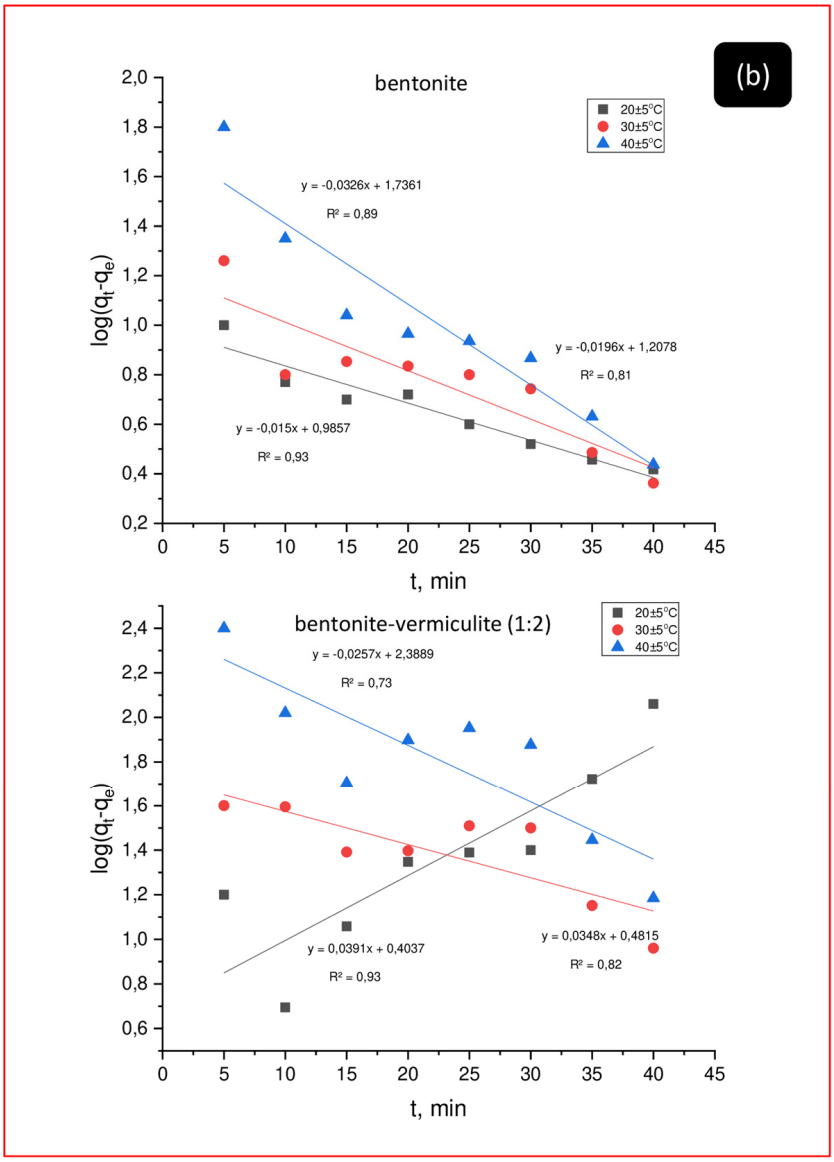

Figure 10. Kinetic model plots for petroleum product absorption on the bentonite and bentonite–vermiculite composite at 20 ± 5, 30 ± 5, and 40 ± 5 °C, fitted with PFO (**a**) and PSO (**b**) models.

Table 5. Rate constants of oil products sorption on bentonite and bentonite–vermiculite mixture at different temperatures.

Model	T, (K)	Values	
		Bentonite	Bentonite–Vermiculite Mixture
Pseudo first-order k (min^{-1})	293	9.96×10^{-2}	3.79×10^{-2}
	303	9.63×10^{-2}	7.57×10^{-2}
	313[2]	8.76×10^{-2}	8.46×10^{-2}
Pseudo second-order k ($g/mg \cdot min^{-1}$)	293	2.89×10^{-4}	5.13×10^{-4}
	303	2.67×10^{-4}	3.57×10^{-5}
	313[2]	1.03×10^{-3}	1.80×10^{-4}

A survey of the literature indicates that the PSO equation often provides a good representation of kinetic adsorption data, for example, for the uptake of the water-soluble fraction (WSF) of diesel fuel on organozeolite [50]. Similarly, for crude oil–in–saline water emulsions, Bahia et al. reported that the PSO model better describes higher-concentration

emulsions, whereas the PFO model may capture low-concentration conditions; importantly, their thermodynamic interpretation suggests that the process is predominantly governed by physisorption [51]. Therefore, an improved PSO fit alone should not be regarded as conclusive evidence of chemisorption. In studies addressing the use of mineral sorbents for petroleum product removal, numerous cases have likewise been reported in which PSO is identified as the most suitable kinetic model alongside conventional isotherm approaches [52,53]. At the same time, PFO-type behavior has also been documented for bentonite-containing systems, where uptake is largely controlled by physisorption and mass-transfer limitations rather than by an idealized surface-reaction step [54,55].

At room temperature (293 K, (20 °C)), the thermodynamic parameters indicate that incorporating vermiculite into the bentonite–vermiculite mixture (1:2) renders the process thermodynamically more favorable, as reflected by the Gibbs free energy of activation (ΔG) for binding water-dissolved hydrocarbon contaminants on the sorbent surface. The ΔG values for the bentonite–vermiculite mixture are close to zero and formally negative for the PSO-based evaluation, whereas for pristine bentonite within the PFO model ΔG remains positive. The entropy of activation (ΔS) suggests opposite trends: for bentonite PFO, $\Delta S < 0$ points to a more ordered transition state, consistent with immobilization of petroleum fractions and the formation of a structured adsorption layer; in contrast, the positive ΔS values obtained for bentonite PSO and for the bentonite–vermiculite mixture PFO imply an entropically favorable contribution, which may be associated with reorganization of the hydration shell and redistribution of the sorbate within the more complex composite structure. Based on the sign of ΔH at 293 K, bentonite PFO exhibits an exothermic character, whereas the bentonite–vermiculite mixture PFO and bentonite PSO display an endothermic contribution, in line with an increased role of transport and structural-rearrangement steps in the composite sorbent. Overall, in the 20–25 °C range the bentonite–vermiculite mixture shows the "softest" thermodynamic profile in terms of ΔG, highlighting its practical promise for petroleum product sorption without additional heating (Table 6).

Table 6. Apparent activation energy (E_a) and thermodynamic parameters (ΔS°, ΔH°, and ΔG°) obtained from PFO and PSO kinetic fits for petroleum product sorption on bentonite and the bentonite–vermiculite mixture at 293–313 K.

Sorbent	Kinetic Model	E_a (kJ·mol^{-1})	T (K)	ΔS (J·mol^{-1}·K^{-1})	ΔH (J·mol^{-1})	ΔG (J·mol^{-1})
Bentonite	Pseudo-first-order (PFO)	−4.882	293	−0.0670	−9.754	2.858
			303	−0.0325	88.450	−26.802
			313	−0.0320	−5.168	1.617
Bentonite	Pseudo-second-order (PSO)	47.730	293	0.0610	42.857	−0.122
			303	−0.0301	−918.929	−24.629
			313	−0.0320	−5.297	0.009
Bentonite + vermiculite	Pseudo-first-order (PFO)	31.856	293	0.0475	25.984	0.003
			303	−0.0303	−595.843	−14.675
			313	−0.0320	−5.283	1.32×10^{-5}
Bentonite + vermiculite	Pseudo-second-order (PSO)	−41.636	293	−0.2421	−46.507	-9.19×10^{-5}
			303	−0.0350	792.161	11.625
			313	−0.0320	−4.994	-3.20×10^{-5}

In this context, the bentonite results-characterized by an exothermic enthalpy term ($\Delta H < 0$ at 293 K under the PFO treatment) and a negative entropy change ($\Delta S < 0$)-indicate that the uptake is primarily governed by physisorption and is accompanied by increased ordering at the solid–liquid interface (i.e., formation of a more structured adsorbed layer). This reading is consistent with the observations reported by Bahia et al. for oil-containing aqueous systems, where physisorption is likewise reflected in a "less random" thermodynamic profile [52]. Obradović et al. reported that hydrocarbon uptake by

organoclays increases with greater interlayer expansion and a more favorable organization of the modifier within the clay structure [56,57]. This finding supports our hypothesis that introducing layered vermiculite into bentonite can enhance petroleum uptake by generating more effective interlayer and surface sorption domains, without requiring chemical modification of the sorbent. The calculated activation energy values are in good agreement with those reported in the literature [58]. Notably, the activation energy of bentonite is approximately an order of magnitude different from that of the composite, indicating that composite formation substantially alters the interfacial energetics and is associated with a more energetically demanding surface process.

3.5. Thermal Behavior

Thermogravimetric analysis was employed to assess the thermal behavior of the sorbents and to quantify mass losses associated with dehydration, desorption, and the thermal decomposition of retained petroleum products. Measurements were conducted from 10 to 1300 °C, and the results are summarized in Figure 11 and Table 7.

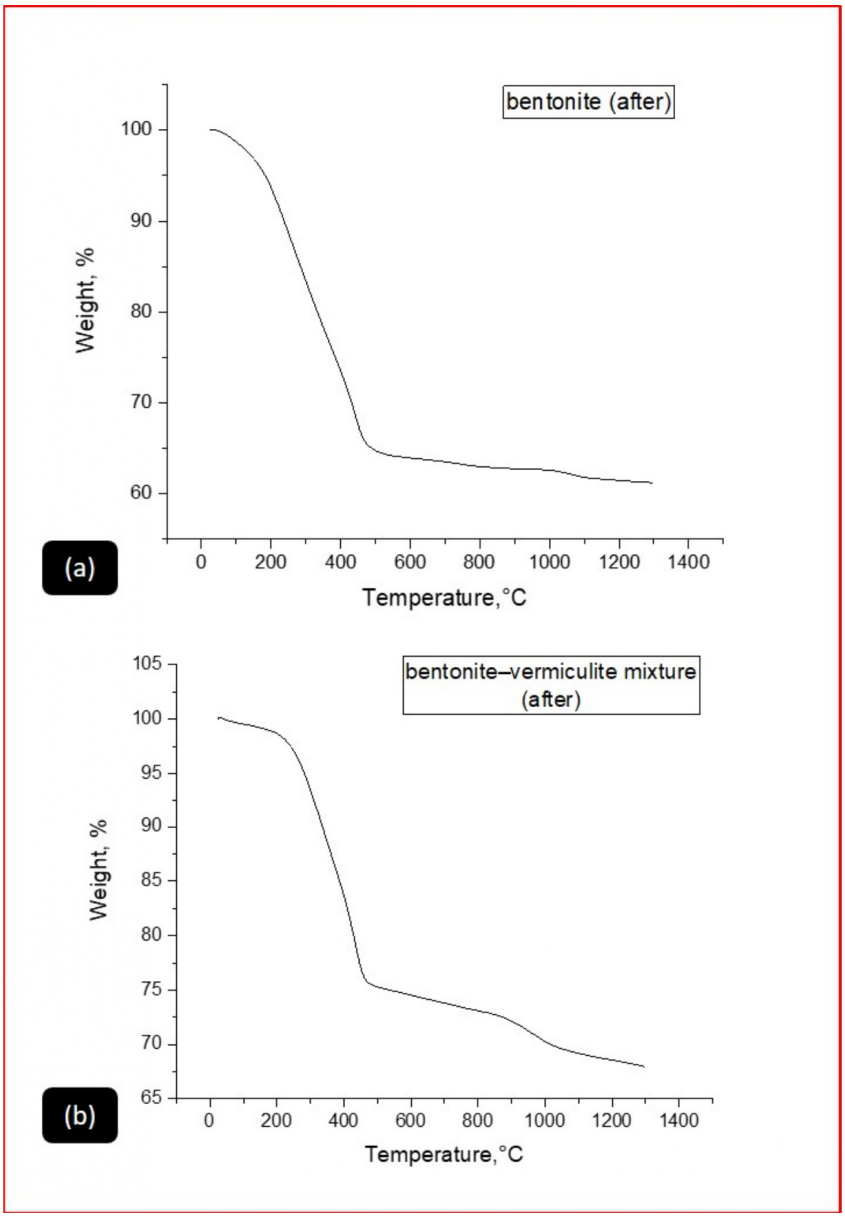

Figure 11. TG curves of sorbents after sorption: (**a**) bentonite; (**b**) bentonite–vermiculite mixture (1:2).

Table 7. Thermogravimetric analysis (TGA) results for bentonite (b) and bentonite–vermiculite composite (b + v) before and after sorption.

Sample	Total Mass Loss (10–1300 °C), %	Residual Mass at 1300 °C, %
b (initial)	6.31	93.68
b (after)	38.78	61.21
b + v (initial)	6.59	93.40
b + v (after)	32.04	67.95

For oil-loaded bentonite (Figure 11a, Table 7), the TG curve exhibits a pronounced overall weight decrease, corresponding to a total mass loss of 38.79% and a residual mass of 61.21% at 1300 °C. The profile is characterized by a dominant mass-loss step at intermediate temperatures, followed by a slow, gradual decline toward high temperatures. This behavior is consistent with the progressive removal of the sorbed petroleum fraction through volatilization and thermal decomposition of hydrocarbons, together with overlapping contributions from bound water release and intrinsic clay transformations (e.g., dehydroxylation) occurring at elevated temperatures. For the oil-loaded bentonite–vermiculite composite (Figure 11b, Table 7), the mass loss is also substantial but lower than that of bentonite, reaching 32.04% with a residual mass of 67.96% at 1300 °C. While the general curve shape remains similar, the higher final residue and reduced total loss indicate that the composite either retains a slightly smaller net amount of oil under the same conditions and/or immobilizes a larger fraction in a thermally more persistent form, reflecting stronger confinement and interfacial interactions within the composite's heterogeneous surface and interlayer domains. A side-by-side evaluation of the TGA results shows that oil uptake causes a substantial rise in mass loss for both sorbents, consistent with the accumulation of an organic fraction. However, after sorption the bentonite–vermiculite composite retains a higher residual mass and undergoes a smaller total mass loss than bentonite, suggesting the formation of adsorption complexes with greater thermal stability. This behavior likely reflects synergistic effects between the composite constituents, a higher density of effective sorption sites, and a more homogeneous incorporation of petroleum compounds within the sorbent structure.

Following oil uptake, both sorbents exhibit a marked rise in total mass loss (38.79% for bentonite and 32.04% for the composite), which can be ascribed to the progressive volatilization/oxidative decomposition of the retained hydrocarbon fraction over a wide temperature interval. In spite of this common trend, the bentonite–vermiculite composite leaves a higher final residue (67.96% vs. 61.21%) and shows a lower overall loss than oil-loaded bentonite. This difference can be rationalized by considering the high-temperature response of vermiculite reported by Balima et al., who demonstrated that compressed K-vermiculite undergoes densification and a concomitant reduction in porosity upon heating above ~800 °C [58]. Such structural evolution may reduce mass-transport pathways for oxygen and volatiles at late stages of heating and enhance confinement of heavier hydrocarbon fractions within the evolving mineral domains, leading to an increased apparent residue-without implying the formation of new crystalline phases within the clay framework [59,60].

Figure 12 presents the DSC curves of the oil-loaded sorbents, b (after) and b + v (after), recorded under nitrogen. Compared with the pristine materials (Table 8), b (after) shows a shift in the main endothermic event to higher characteristic temperatures ($T_{Onset} \approx 359$ °C; $T_{Peak\_} \approx 407$ °C) accompanied by a lower enthalpy ($\Delta H = 41.7$ kJ·g^{-1}), which is consistent with partial replacement of bound water by the sorbed petroleum phase and a reduced dehydration contribution, while the remaining heat-flow response reflects thermally driven transformations of the retained organic fraction [60–62]. Ther-

mal analysis studies commonly distinguish water desorption at lower temperatures from organic-matter degradation at higher temperatures in clay-containing systems, supporting this coupled interpretation of dehydration and organic-fraction transformations [61]. By contrast, b + v (after) exhibits a much stronger and broadened high-temperature event spanning 360–545 °C, with $T_{Peak} \approx 470$ °C and a markedly higher enthalpy ($\Delta H = 141.6$ kJ·g^{-1}, Table 8), indicating a more energy-demanding transformation pathway for the retained petroleum fraction and stronger interfacial association within the composite's heterogeneous surface and interlayer domains. This behavior aligns with reports that clays interacting with multiple organic fractions can produce enhanced and distributed thermal signals in the organic-degradation region, reflecting mineral–organic synergy and a broader spectrum of thermally stable bound organics. Importantly, vermiculite is expected to remain structurally robust over this temperature interval, while its most pronounced structural and textural evolution (densification with reduced porosity) is reported to occur only above ~800 °C; therefore, the intensified DSC response of b + v (after) up to 545 °C is most plausibly governed by the retained hydrocarbons and their interfacial binding rather than by vermiculite framework breakdown [58]. Overall, the DSC comparison indicates that incorporating vermiculite into bentonite promotes the formation of thermally more persistent mineral–organic associations after sorption, consistent with stronger confinement and a wider distribution of interaction environments for petroleum-derived species.

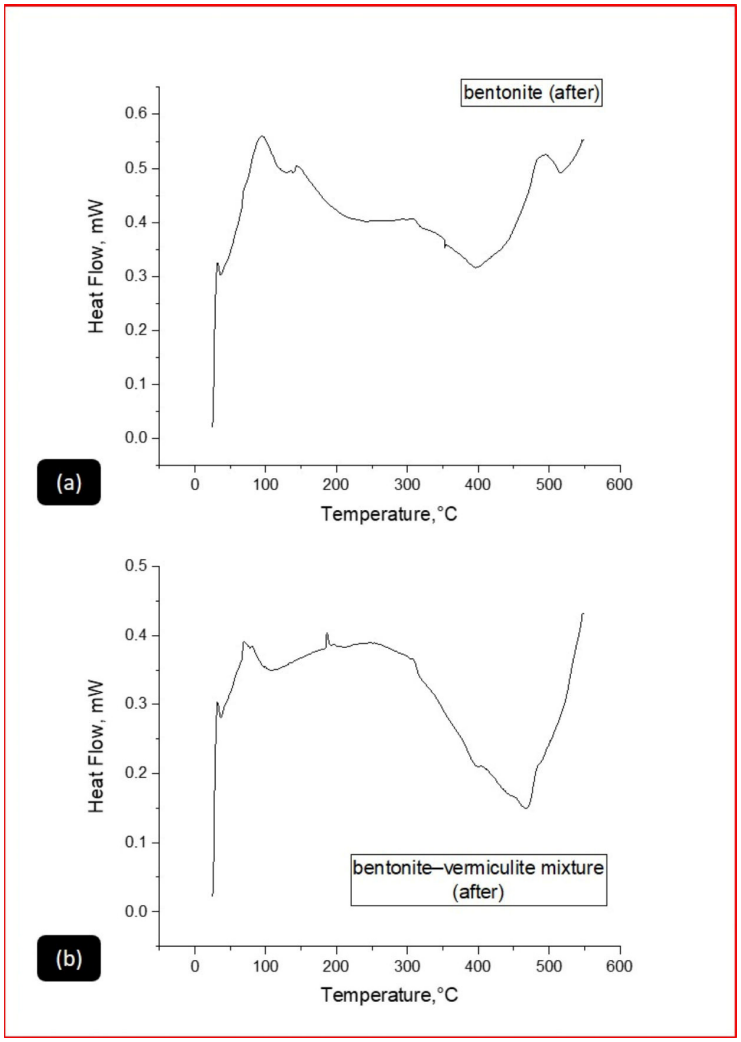

Figure 12. DSC curves of bentonite (**a**) and bentonite–vermiculite (**b**) sorbents before and after sorption.

Table 8. DSC transition parameters for bentonite and bentonite–vermiculite sorbents before and after sorption.

Sample	T_{onset} (°C)	T_{peak} (°C)	T_{endset} (°C)	ΔH (kJ·g^{-1})
b (initial)	250	375	467	74.64
b (after)	359	407	474	41.73
b + v (initial)	317	353	382	2.00
b + v (after)	361	470	545	141.59

3.6. Technological Performance and Techno-Economic Assessment

To assess the economic feasibility of adsorption-based treatment of oil-contaminated wastewater using a bentonite–vermiculite mixture, the required amount of sorbent was calculated based on the initial parameters presented in Table 9. The process throughput and wastewater flow rate (Q = 120,000 L·h^{-1}) were adopted from real operational data of industrial facilities and correspond to the values previously reported in [23]. This flow rate corresponds to the typical wastewater volumes encountered at petrochemical installations in Kazakhstan and was therefore used as a realistic baseline parameter for calculating sorbent dosages and assessing the technological efficiency of the adsorption treatment process.

Table 9. Input parameters for calculating the amount of adsorbent material required for multistage treatment of oil-contaminated wastewater.

Parameter, Units	Value
Throughput, Q (m^3·h^{-1}(m^3·s^{-1}))	120 (0.033)
Adsorption capacity, *a* (mg O_2·g^{-1})	19.6
Initial oil concentration, C_0 (mg/L)	392
Final oil concentration, C_k (mg/L)	0.35

Note: Values in parentheses correspond to units converted to SI (m^3·s^{-1}).

The input parameters used for the techno-economic calculations are summarized in Table 9, while the calculated technological and performance indicators are presented in Table 10.

Table 10. Calculated technological indicators for multistage adsorption treatment.

Parameter, Units	Value
Adsorption coefficient, k	56
Required adsorbent mass (single stage), m (kg)	2397
Number of adsorption stages, n	1
Total adsorbent consumption, m_0 (t)	12.38
Annual adsorbent consumption, P (kg·year^{-1})	2618
Annual cost adsorbent, Z (thousand USD)	389,658
Specific treatment cost, $Z_{1\ m3}$ (USD·m^{-3})	0.15
Estimated economic damage reduction, D (USD)	5,355,726

Note: All calculated indicators were obtained using Equations (17)–(26) based on the input parameters summarized in Table 9.

The results of the technological calculations demonstrate that the bentonite–vermiculite mixture can be effectively applied to reduce the concentration of oil contaminants in wastewater from an initial value of 392 mg·L^{-1} to 0.35 mg·L^{-1}. This concentration range is typical for wastewater generated by oil-refining and petrochemical facilities and is described in the literature as difficult to remove due to the presence of stable emulsified oil forms [63].

The specific adsorption capacity depends on the material modification. A specific adsorption capacity of 19.6 mg $O_2 \cdot g^{-1}$ reflects the oil uptake capability of natural layered materials based on bentonite and vermiculite [64].

The calculation of the adsorption coefficient k and the number of treatment stages n made it possible to describe the dynamics of oil concentration reduction during adsorbent addition. The value of n indicates surface heterogeneity characteristic of mineral sorbents and the formation of multisite adsorption, which is consistent with the Freundlich adsorption model. An n-value below unity suggests a high affinity of the adsorbent toward organic pollutants and gradual surface saturation with increasing adsorbent dosage [65,66].

The main advantages of the bentonite–vermiculite mixture are its chemical stability, low cost, and environmental safety compared to synthetic adsorbents. Natural materials demonstrate high stability under real wastewater conditions, making them more suitable for industrial applications [67,68]. The obtained values indicate the feasibility of economically justified operation of the treatment system with a throughput of 120,000 $L \cdot h^{-1}$, which is consistent with the conclusions reported by [69].

An important aspect of the economic efficiency of the composite lies in its enhanced sorption performance, which reduces the required sorbent mass and the frequency of its replacement. The sorbent exhibited both physical stability and chemical selectivity due to the synergistic effect of bentonite and vermiculite, which are known for their high specific surface area, cation-exchange capacity, and hydrophobic interactions with petroleum compounds. Similar properties have been reported in studies evaluating the performance of modified mineral adsorbents for oil-contaminated wastewater treatment [70,71].

The conducted techno-economic analysis demonstrated the high efficiency and feasibility of using the bentonite–vermiculite composite for the treatment of oil-contaminated wastewater. In particular, the protective sorbent layer retained its activity for 51 h, while the annual material consumption amounted to 2618 tonnes, indicating good industrial scalability and operational reliability.

The cost assessment of sorbent production indicates that the total required expenditure amounts to USD 389,658. The unit cost of wastewater treatment is estimated at USD 0.15 per m^3. The obtained values demonstrate that the bentonite–vermiculite composite sorbent is more economically efficient than many conventional sorbents, including activated carbon. Yasir et al. (2024) reported that the average treatment cost using activated carbon ranges from USD 0.70 to 1.20 per m^3, whereas biochar-based sorbents exhibit an economic efficiency of approximately EUR 0.89 per m^3 under optimized reuse conditions [70,72].

In addition, the assessment of the potential environmental damage indicates that oil contamination of water bodies could result in losses exceeding USD 5,355,726. These findings emphasize the economic feasibility of employing the proposed adsorbents in wastewater treatment systems. The obtained results are consistent with previous techno-economic evaluations demonstrating that low-cost adsorbents can provide both economic efficiency and environmental justification when applied at large scale [73,74].

Overall, the performed calculations demonstrate the high technological efficiency of adsorption-based wastewater treatment for oil removal using the bentonite–vermiculite mixture. The application of the proposed composite adsorbent not only ensures economic effectiveness but also contributes to a reduction in anthropogenic environmental impact, confirming its suitability for practical use in environmental engineering and pollution control.

4. Conclusions

This study demonstrates that the bentonite–vermiculite composite (1:2 mass ratio) is an effective and environmentally benign mineral sorbent for removing petroleum products

from contaminated water. Adsorption equilibrium, kinetic, and thermodynamic analyses indicate that oil uptake is mainly governed by physisorption and ion exchange and is well described by the PSO model. SEM/EDS and XRD confirmed preservation of the layered aluminosilicate structure after adsorption, while ζ-potential and DLS revealed controlled surface charge attenuation and aggregation behavior associated with hydrocarbon binding. TGA/DSC results supported strong sorbate–sorbent interactions and maintained thermal stability of the oil-loaded materials. Techno-economic assessment under industrially relevant conditions confirmed process feasibility and cost efficiency, achieving effective oil removal at a low treatment cost. Overall, the 1:2 composite ratio is suitable for industrial wastewater treatment and offers potential for cyclic utilization within a resource-efficient circular process concept.

Author Contributions: Conceptualization, D.B. and N.A.; methodology, D.B. and N.A.; investigation, G.L., A.B. and S.N.; formal analysis, A.B. and G.L.; data curation, A.B.; visualization, A.B. and G.A.; validation, G.L. and A.B.; writing—original draft preparation, D.B. and N.A.; writing—review and editing, N.A.; supervision, D.B.; project administration, D.B.; resources, D.B., G.A. and S.N.; funding acquisition, N.A. and G.A. All authors have read and agreed to the published version of the manuscript.

Funding: This research is funded by the Committee of Science of the Ministry of Science and Higher Education of the Kazakhstan (Grant No. BR24992882 Development of new technologies for processing man-made waste with improvement of the environmental situation in the region).

Data Availability Statement: The original contributions presented in this study are included in the article. Further inquiries can be directed to the corresponding author.

Acknowledgments: The authors acknowledge the administrative and technical support provided during the course of this study. During the preparation of this manuscript, the authors used ChatGPT (OpenAI, GPT-5.2) solely for linguistic and stylistic assistance. The authors critically reviewed and edited the content and accept full responsibility for the final version of the manuscript.

Conflicts of Interest: The authors declare no conflict of interest.

References

1. Al-Najar, J.A.; Al-Humairi, S.T.; Lutfee, T.; Balakrishnan, D.; Veza, I.; Soudagar, M.E.M.; Fattah, I.M.R. Cost-Effective Natural Adsorbents for Remediation of Oil-Contaminated Water. *Water* **2023**, *15*, 1186. [CrossRef]
2. Bandura, L.; Woszuk, A.; Kołodyńska, D.; Franus, W. Application of Mineral Sorbents for Removal of Petroleum Substances: A Review. *Minerals* **2017**, *7*, 37. [CrossRef]
3. Kumari, S.; Chowdhry, J.; Kumar, M.; Garg, M.C. Zeolites in Wastewater Treatment: A Comprehensive Review on Scientometric Analysis, Adsorption Mechanisms, and Future Prospects. *Environ. Res.* **2024**, *260*, 119782. [CrossRef] [PubMed]
4. Dabizha, O.N.; Khamova, T.V.; Shilova, O.A. Mechanochemical Modification of Zeolite Rocks with Polyacrylamide for the Preparation of Oil Sorbents. *Inorg. Mater.* **2023**, *59*, 1127–1139. [CrossRef]
5. Lepesbayeva, G.; Belgibayeva, D.; Amerkhanova, S.; Biktasova, A.; Aikenova, N.; Abilova, G. Surface characterization of a bentonite–vermiculite mixture as a cost-effective adsorbents for oil removal from water. *Results Chem.* **2025**, *18*, 102838. [CrossRef]
6. Baskar, A.V.; Bolan, N.; Hoang, S.A.; Sooriyakumar, P.; Kumar, M.; Singh, L.; Jasemizad, T.; Padhye, L.P.; Singh, G.; Vinu, A.; et al. Recovery, Regeneration and Sustainable Management of Spent Adsorbents from Wastewater Treatment Streams: A Review. *Sci. Total Environ.* **2022**, *822*, 153555. [CrossRef]
7. Wang, X.; Dong, H.; Zhang, Z.; Xie, H. Melamine-Modified Bentonite Nanocomposites for Selective Removal of Hg(II) Ions: Preparation, Characterization, and Mechanism. *Colloids Surf. A Physicochem. Eng. Asp.* **2025**, *733*, 139237. [CrossRef]
8. Murray, H.H. Overview—Clay Mineral Applications. *Appl. Clay Sci.* **1991**, *5*, 379–395. [CrossRef]
9. Yliharju, J.; Harjupatana, T.; Kuva, J.; Reijonen, H.; Kataja, M.; Miettinen, A. Observation of Water Transport in Compacted Bentonite at Elevated Temperatures Using X-ray Tomography and Image Analysis. *Geomech. Energy Environ.* **2025**, *44*, 100767. [CrossRef]
10. Okiel, K.; El-Sayed, M.; El-Kady, M.Y. Treatment of Oil–Water Emulsions by Adsorption onto Activated Carbon, Bentonite and Deposited Carbon. *Egypt. J. Pet.* **2011**, *20*, 9–15. [CrossRef]

11. Alvarez-Silva, M.; Uribe-Salas, A.; Mirnezami, M.; Finch, J.A. The Point of Zero Charge of Phyllosilicate Minerals Using the Mular–Roberts Titration Technique. *Miner. Eng.* **2010**, *23*, 383–389. [CrossRef]
12. Goh, R.; Leong, Y.-K.; Lehane, B. Bentonite Slurries—Zeta Potential, Yield Stress, Adsorbed Additive and Time-Dependent Behaviour. *Rheol. Acta* **2011**, *50*, 29–38. [CrossRef]
13. Au, P.-I.; Leong, Y.-K. Rheological and Zeta Potential Behaviour of Kaolin and Bentonite Composite Slurries. *Colloids Surf. A Physicochem. Eng. Asp.* **2013**, *436*, 530–541. [CrossRef]
14. Marouf, R.; Marouf-Khelifa, K.; Schott, J.; Khelifa, A. Zeta Potential Study of Thermally Treated Dolomite Samples in Electrolyte Solutions. *Microporous Mesoporous Mater.* **2009**, *122*, 99–104. [CrossRef]
15. Delgado, A.V.; González-Caballero, F.; Hunter, R.J.; Koopal, L.K.; Lyklema, J. Measurement and Interpretation of Electrokinetic Phenomena (IUPAC Technical Report). *Pure Appl. Chem.* **2005**, *77*, 1753–1805. [CrossRef]
16. Nguyen, D.C.; Bui, T.T.; Cho, Y.B.; Kim, Y.S. Highly Hydrophobic Polydimethylsiloxane-Coated Expanded Vermiculite Sorbents for Selective Oil Removal from Water. *Nanomaterials* **2021**, *11*, 367. [CrossRef]
17. Henry, D.C. The Cataphoresis of Suspended Particles. Part I.—The Equation of Cataphoresis. *Proc. R. Soc. Lond. A* **1931**, *133*, 106–129. [CrossRef]
18. O'Brien, R.W.; White, L.R. Electrophoretic Mobility of a Spherical Colloidal Particle. *J. Chem. Soc. Faraday Trans. 2* **1978**, *74*, 1607–1626. [CrossRef]
19. Grahame, D.C. The Electrical Double Layer and the Theory of Electrocapillarity. *Chem. Rev.* **1947**, *41*, 441–501. [CrossRef]
20. Bergaya, F.; Lagaly, G. (Eds.) *Handbook of Clay Science*, 2nd ed.; Elsevier: Amsterdam, The Netherlands, 2013; ISBN 978-0-08-099364-5.
21. Wang, C.; Boithias, L.; Ning, Z.; Han, Y.; Sauvage, S.; Sánchez-Pérez, J.-M.; Kuramochi, K.; Hatano, R. Comparison of Langmuir and Freundlich Adsorption Equations within the SWAT-K Model for Assessing Potassium Environmental Losses at Basin Scale. *Agric. Water Manag.* **2017**, *180*, 205–211. [CrossRef]
22. Azizian, S. Kinetic models of sorption: A theoretical analysis. *J. Colloid Interface Sci.* **2004**, *276*, 47–52. [CrossRef] [PubMed]
23. Atkins, P.; de Paula, J.; Keeler, J. *Atkins' Physical Chemistry*, 11th ed.; Oxford University Press: Oxford, UK, 2018.
24. Aikenova, N.; Sarsembim, U.; Almuratova, K. Wastewater Treatment of Industrial Enterprises from Phenols with Modified Carbonate Sludge. *Evergreen* **2023**, *10*, 2244–2254. [CrossRef] [PubMed]
25. Darla, U.; Lataye, D.; Kumar, A.; Pandit, B.; Ubaidullah, M. Adsorption of Phenol Using Adsorbent Derived from *Saccharum officinarum* Biomass: Optimization, Isotherms, Kinetics, and Thermodynamic Study. *Sci. Rep.* **2023**, *13*, 42461. [CrossRef] [PubMed]
26. Zhao, M.-Q.; Huang, J.-Q.; Zhang, Q.; Luo, W.-L.; Wei, F. Improvement of Oil Adsorption Performance by a Sponge-Like Natural Vermiculite–Carbon Nanotube Hybrid. *Appl. Clay Sci.* **2011**, *53*, 1–7. [CrossRef]
27. Huang, K.; Rowe, P.; Chi, C.; Sreepal, V.; Bohn, T.; Zhou, K.-G.; Su, Y.; Prestat, E.; Pillai, P.B.; Cherian, C.T.; et al. Cation-Controlled Wetting Properties of Vermiculite Membranes and Its Promise for Fouling Resistant Oil–Water Separation. *Nat. Commun.* **2020**, *11*, 1097. [CrossRef]
28. Hunter, R.J. *Zeta Potential in Colloid Science: Principles and Applications*; Academic Press: London, UK, 1981; pp. 219–257. [CrossRef]
29. Mostafa, H.; Zaher, A.; Seliem, M.K.; Shehata, N. New Insights into the Management of Hard Water Using Bentonite: Experimental and Statistical Physics Treatment. *Water Pract. Technol.* **2025**, *20*, 67. [CrossRef]
30. Barloková, D.; Marton, M. Removal of Selected Pesticides from Water Using Granular Activated Carbon. *IOP Conf. Ser. Earth Environ. Sci.* **2021**, *900*, 012011. [CrossRef]
31. Ali, M.; Asim, M.; Khan, T.A. Low Cost Adsorbents for the Removal of Organic Pollutants from Wastewater. *J. Environ. Manag.* **2012**, *113*, 170–183. [CrossRef]
32. Pereira, A.; Freitas, A.; Silva, M.; Camara, A.; Moura, H.; Ballesteros-Plata, D.; Rodríguez-Castellón, E.; de Carvalho, L. Efficient Removal of Tetracycline Hydrochloride via Adsorption onto Modified Bentonite: Kinetics and Equilibrium Studies. *Appl. Sci.* **2025**, *15*, 3372. [CrossRef]
33. Kasemodel, M.C.; de Aguiar, L.G.; Rodrigues, V.G.S.; Romão, É.L. The Investigation of the Adsorption of Methylene Blue from Water by Torrefied Biomass. *Colorants* **2025**, *4*, 21. [CrossRef]
34. Food and Agriculture Organization of the United Nations (FAO); World Health Organization (WHO). Activated Carbon. FAO JECFA Monographs, 10. 2010. Available online: https://www.fao.org/3/i1580e/i1580e.pdf (accessed on 30 November 2025).
35. Hoslett, J.; Ghazal, H.; Mohamad, N.; Jouhara, H. Removal of methylene blue from aqueous solutions by biochar prepared from the pyrolysis of mixed municipal discarded material. *Sci. Total Environ.* **2020**, *714*, 136832. [CrossRef] [PubMed]
36. Tang, S.; Wang, Y.; He, P.; Wang, Y.; Wei, G. Recent Advances in Metal–Organic Framework (MOF)-Based Composites for Organic Effluent Remediation. *Materials* **2024**, *17*, 2660. [CrossRef] [PubMed]
37. Sun, W.-J.; Tang, Q.-T.; Lu, T.-H.; Fan, R.-D.; Sun, G.-G.; Tan, Y.-Z. Adsorption Performance of Bentonite and Clay for Zn(II) in Landfill Leachate. *Geoenviron. Disasters* **2024**, *11*, 4. [CrossRef]

38. Hamad, H.N.; Idrus, S.; Yusuf, B.; Jamali, N.S.; Ahsan, A.; Suhartini, S.; Wahab, A.M.A. Optimized Bentonite Clay Adsorbents for Methylene Blue Removal. *Processes* **2024**, *12*, 738. [CrossRef]
39. Dlamini, L.N. Study of Adsorption Properties of Bentonite Clay. In *Bentonite Clay: Environmental Properties and Applications*; IntechOpen: London, UK, 2020. [CrossRef]
40. Al-Rashdi, B.; Johnson, D.J.; Hilal, N. Adsorptive Removal of Heavy Metals and Dyes from Water Using Clay-Based Adsorbents: A Review. In *Montmorillonite: Properties, Characteristics, and Its Harnessing in Environmental Applications*; IntechOpen: London, UK, 2023. [CrossRef]
41. Paredes-Laverde, M.; Martínez, D.F.; Torres-Palma, R.A. Montmorillonite-Based Natural Adsorbent from Colombia for the Removal of Organic Pollutants from Water: Isotherms, Kinetics, Nature of Pollutants, and Matrix Effects. *Water* **2023**, *15*, 1046. [CrossRef]
42. Zhou, H.; Chen, M.; Zhu, R.; Lu, X.; Zhu, J. Coupling between Clay Swelling/Collapse and Cationic Partition. *Geochim. Cosmochim. Acta* **2020**, *285*, 78–99. [CrossRef]
43. Zhang, L.; Lu, X.; Liu, X.; Zhou, J.; Zhou, H. Hydration and Mobility of Interlayer Ions of (Na_x, Ca_γ)-Montmorillonite: A Molecular Dynamics Study. *J. Phys. Chem. C* **2014**, *118*, 29811–29821. [CrossRef]
44. Chen, W.L.; Grabowski, R.C.; Goel, S. Clay Swelling: Role of Cations in Stabilizing/Destabilizing Mechanisms. *ACS Omega* **2022**, *7*, 3185–3191. [CrossRef]
45. Lantenois, S.; Champallier, R.; Bény, J.-M.; Muller, F. Hydrothermal Synthesis and Characterization of Dioctahedral Smectites: A Montmorillonites Series. *Appl. Clay Sci.* **2008**, *38*, 165–178. [CrossRef]
46. Moraes, D.S.; Miranda, L.C.R.; Angélica, R.S.; Filho, G.N.R.; Zamian, J.R. Functionalization of Bentonite and Vermiculite after the Creation of Structural Defects through an Acid Leaching Process. *J. Braz. Chem. Soc.* **2018**, *29*, 320–327. [CrossRef]
47. Emmerich, K.; Wolters, F.; Kahr, G.; Lagaly, G. Clay Profiling: The Classification of Montmorillonites. *Clays Clay Miner.* **2009**, *57*, 104–114. [CrossRef]
48. Li, C.; Fu, L.; Ouyang, J.; Yang, H. Enhanced Performance and Interfacial Investigation of Mineral-Based Composite Phase Change Materials for Thermal Energy Storage. *Sci. Rep.* **2013**, *3*, 1908. [CrossRef]
49. Kim, M.; Kwon, D.K.; Kim, H.; Park, W.; Cha, B.; Yea, Y.; Yoon, Y.; Elanchezhiyan, S.S.D.; Park, C.M. Waste PU-Derived PDMS/ZIF-8/Bentonite Composite Sponge for Reusable Oil Sorption. *J. Hazard. Mater. Lett.* **2026**, *7*, 100175. [CrossRef]
50. Fajdek-Bieda, A.; Wróblewska, A.; Piz, M. Vermiculite as an Eco-Friendly Catalyst in the Isomerization and Cyclization of Geraniol: Optimization Using the Response Surface Method. *Molecules* **2025**, *30*, 4113. [CrossRef] [PubMed]
51. Ezzati, R. Derivation of Pseudo-First-Order, Pseudo-Second-Order and Modified Pseudo-First-Order Rate Equations from Langmuir and Freundlich Isotherms for Adsorption. *Chem. Eng. J.* **2020**, *392*, 123705. [CrossRef]
52. Lukić, M.; Daković, A.; Joksimović, K.; Milić, J.; Obradović, M.; Beškoski, V.; Avdalović, J. Removal of Diesel from Aqueous Solutions by a Combined Adsorption and Microbial Degradation Process. *Minerals* **2024**, *14*, 1287. [CrossRef]
53. Bahia, P.V.B.; Ferreira, G.A.; Mascarenhas, A.J.S.; Castro, F.D.S.; Fréty, R.T.F.; Vidal, R.R.L. Sustainable Treatment of Crude Oil-in-Saline Water Emulsion with Licuri (*Syagrus coronata*) Leaf Fiber. *Sustainability* **2025**, *17*, 7188. [CrossRef]
54. Shahzadi, F.; Sun, X.-F.; Sheraz, M. Sustainable Cellulose–Bentonite Composites for Wastewater Treatment. *Materials* **2025**, *18*, 4284. [CrossRef]
55. Kostoglou, M.; Karapantsios, T.D. Why Is the Linearized Form of Pseudo-Second Order Adsorption Kinetic Model So Successful in Fitting Batch Adsorption Experimental Data? *Colloids Interfaces* **2022**, *6*, 55. [CrossRef]
56. Tran, H.N. Applying Linear Forms of Pseudo-Second-Order Kinetic Model for Feasibly Identifying Errors in the Initial Periods of Time-Dependent Adsorption Datasets. *Water* **2023**, *15*, 1231. [CrossRef]
57. Obradović, M.; Daković, A.; Smiljanić, D.; Marković, M.; Ožegović, M.; Krstić, J.; Vuković, N.; Milojević-Rakić, M. Bentonite Modified with Surfactants—Efficient Adsorbents for the Removal of Non-Steroidal Anti-Inflammatory Drugs. *Processes* **2024**, *12*, 96. [CrossRef]
58. de Carvalho Arjona, J.; Sousa, P.H.; Demarquette, N.R.; Valenzuela-Diaz, F.R. Transforming Bentonite into High Sorption Capacity Organoclays for Gasoline, Diesel, and Kerosene. *Minerals* **2026**, *16*, 14. [CrossRef]
59. Balima, F.; Nguyen, A.-N.; Reinert, L.; Le Floch, S.; Pischedda, V.; Duclaux, L.; San-Miguel, A. Effect of the Temperature on the Structural and Textural Properties of a Compressed K-Vermiculite. *Chem. Eng. Sci.* **2015**, *134*, 555–562. [CrossRef]
60. Quintero -Jaramillo, J.A.; Carrero, J.I.; Sanabria-González, N.R. Caffeine Adsorption on a Thermally Modified Bentonite: Adsorbent Characterization, Experimental Design, Equilibrium and Kinetics. *Colloids Interface* **2024**, *8*, 26. [CrossRef]
61. Šimkovič, I.; Hrabovský, A.; Hamerníková, A.J.; Ihnačáková, S.; Dlapa, P. Thermogravimetric data suggest synergy between different organic fractions and clay in soil structure formation. *Geoderma* **2025**, *454*, 117166. [CrossRef]
62. Yang, S.; Zhang, Q.; Yang, D. Influence of Temperature and Bedding Planes on the Mode I Fracture Toughness and Fracture Energy of Oil Shale Under Real-Time High-Temperature Conditions. *Energies* **2024**, *17*, 5344. [CrossRef]
63. Rad, L.R.; Anbia, M. Zeolite-Based Composites for the Adsorption of Toxic Matters from Water: A Review. *J. Environ. Chem. Eng.* **2021**, *9*, 106088. [CrossRef]

64. Zhang, X.; Chen, Z.; Shen, J.; Zhao, S.; Kang, J.; Chu, W.; Zhou, Y.; Wang, B. Formation and Interdependence of Disinfection Byproducts during Chlorination of Natural Organic Matter in a Conventional Drinking Water Treatment Plant. *Chemosphere* **2020**, *242*, 125227. [CrossRef]
65. Pour, S.E.; Mamaghani, A.H.; Hashisho, Z. Modeling of Adsorption Process on Monolith Adsorbents: A Mini-Review. *Sep. Purif. Technol.* **2025**, *354*, 128846. [CrossRef]
66. Griffith, C.; Daigle, H. A Comparison of the Static and Dynamic Stability of Pickering Emulsions. *Colloids Surf. A Physicochem. Eng. Asp.* **2020**, *586*, 124256. [CrossRef]
67. Hou, H.; Xiao, J.; Zhang, Z.; You, Z.; Yao, Z.; Zhong, Q. Synergy of Mn–Fe–Al and Reconstruction of Chemisorption and Physisorption in Arsenic Removal. *Sep. Purif. Technol.* **2022**, *299*, 121748. [CrossRef]
68. Yeon, T.; Han, H.; Park, E.; Yie, J. Adsorption and Desorption Characteristics of Hydrocarbons in Multi-Layered Hydrocarbon Traps. *Microporous Mesoporous Mater.* **2009**, *119*, 349–355. [CrossRef]
69. Wang, J.; Guo, X. Adsorption Kinetics and Isotherm Models of Heavy Metals by Various Adsorbents: An Overview. *Crit. Rev. Environ. Sci. Technol.* **2023**, *53*, 1837–1865. [CrossRef]
70. Yasir, H.A.; Zein, S.H.; Holliday, M.C.; Jabbar, K.J.; Ahmed, U.; Jalil, A.A. Comparison of Activated Carbon and Low-Cost Adsorbents for Removal of 2,4-Dichlorophenol from Wastewater Using Aspen Adsorption and Response Surface Methodology. *Environ. Technol.* **2024**, *45*, 3029–3047. [CrossRef]
71. Baaloudj, O.; Langerame, F.; Iunnissi, R.; Buttiglieri, G.; Del Buono, D.; Khadhar, S.; Scrano, L.; Trotta, V.; Brienza, M. Biochar-Based Downflow Fixed-Bed Adsorption Systems for Water Treatment: Process Optimization, Reusability, and Techno-Economic Evaluation. *Sep. Purif. Technol.* **2025**, *377*, 134347. [CrossRef]
72. Ighalo, J.O.; Omoarukhe, F.O.; Ojukwu, V.E.; Iwuozor, K.O.; Igwegbe, C.A. Cost of Adsorbent Preparation and Usage in Wastewater Treatment: A Review. *Clean. Chem. Eng.* **2022**, *3*, 100042. [CrossRef]
73. Amari, A.; Osman, H.; Boujelbene, M.; Abdulameer, M.K.; Scholz, M.; Sammen, S.S. Enhancing Oil–Water Separation Efficiency with WO_3/MXene Composite Membrane. *Water* **2024**, *16*, 1767. [CrossRef]
74. Hammouda, S.B.; Chen, Z.; An, C.; Lee, K. Recent Advances in Developing Cellulosic Sorbent Materials for Oil Spill Cleanup: A State-of-the-Art Review. *J. Clean. Prod.* **2021**, *311*, 127630. [CrossRef]